

Article

Petrology, Palynology, and Geochemistry of Gray Hawk Coal (Early Pennsylvanian, Langsettian) in Eastern Kentucky, USA

James C. Hower ^{1,*}, Cortland F. Eble ², Jennifer M. K. O’Keefe ³, Shifeng Dai ⁴, Peipei Wang ⁴, Panpan Xie ⁴, Jingjing Liu ⁴, Colin R. Ward ⁵ and David French ⁵

¹ Center for Applied Energy Research, University of Kentucky, 2540 Research Park Drive, Lexington, KY 40511, USA

² Kentucky Geological Survey, Lexington, KY 40506, USA; E-Mail: eble@uky.edu

³ Department of Earth & Space Science, Morehead State University, Morehead, KY 40351, USA; E-Mail: j.okeefe@moreheadstate.edu

⁴ State Key Laboratory of Coal Resources and Safe Mining, China University of Mining and Technology (Beijing), Beijing 100083, China; E-Mails: daishifeng@gmail.com (S.D.); wangpeipei1100@gmail.com (P.W.); xiepanpan90@163.com (P.X.); liujj.cumtb@gmail.com (J.L.)

⁵ School of Biological, Earth and Environmental Sciences, University of New South Wales, Sydney, NSW 2052, Australia; E-Mails: c.ward@unsw.edu.au (C.R.W.); d.french@unsw.edu.au (D.F.)

* Author to whom correspondence should be addressed; E-Mail: james.hower@uky.edu; Tel.: +1-859-257-0261; Fax: +1-859-257-0360.

Academic Editor: Karen Hudson-Edwards

Received: 13 July 2015 / Accepted: 31 August 2015 / Published: 11 September 2015

Abstract: This study presents recently collected data examining the organic petrology, palynology, mineralogy and geochemistry of the Gray Hawk coal bed. From the Early Pennsylvanian, Langsettian substage, Gray Hawk coal has been mined near the western edge of the eastern Kentucky portion of the Central Appalachian coalfield. While the coal is thin, rarely more than 0.5-m thick, it has a low-ash yield and a low-S content, making it an important local resource. The Gray Hawk coal palynology is dominated by *Lycospora* spp., and contains a diverse spectrum of small lycopods, tree ferns, small ferns, calamites, and gymnosperms. The maceral assemblages show an abundance of collotelinite, telinite, vitrodetrinite, fusinite, and semifusinite. Fecal pellet-derived macrinite, albeit with more compaction than is typically seen in younger coals, was observed in the Gray Hawk coal. The minerals in the coal are dominated by clay minerals (e.g., kaolinite, mixed-layer illite/smectite, illite), and to a lesser extent, pyrite, quartz, and iron III hydroxyl-sulfate,

along with traces of chlorite, and in some cases, jarosite, szomolnokite, anatase, and calcite. The clay minerals are of authigenic and detrital origins. The occurrence of anatase as cell-fillings also indicates an authigenic origin. With the exception of Ge and As, which are slightly enriched in the coals, the concentrations of other trace elements are either close to or much lower than the averages for world hard coals. Arsenic and Hg are also enriched in the top bench of the coal and probably occur in pyrite. The elemental associations (e.g., $\text{Al}_2\text{O}_3/\text{TiO}_2$, Cr/Th-Sc/Th) indicate a sediment-source region with intermediate and felsic compositions. Rare metals, including Ga, rare earth elements and Ge, are highly enriched in the coal ashes, and the Gray Hawk coals have a great potential for industrial use of these metals. The rare earth elements in the samples are weakly fractionated or are characterized by heavy-REE enrichment, indicating an input of natural waters or probably epithermal solutions.

Keywords: trace elements in coal; minerals in coal; epiphyllous fungi; macrinite; Gray Hawk coal

1. Introduction

The Lower Pennsylvanian Langsettian-substage Gray Hawk coal bed (Figure 1) has been mined in a small area in the western part of the Kentucky portion of the Central Appalachian coalfield; the samples considered here are from five 7½-minute quadrangles in three counties (Figure 2). The Gray Hawk coal is one of the uppermost Langsettian (late Westphalian A) coals in the region, with the overlying Lily/Manchester/River Gem (also known by at least 18 other names) coal being the oldest truly widespread coal in eastern Kentucky [1]. Despite its restricted geographic range, the thin coal (with most sites having coal <45.7 cm (<18 inches) thick) has been a valuable local resource owing to its relatively low-ash yield and low-S content, allowing it to be shipped as a run-of-mine coal. (This observation is based on observations by Hower and Eble in their several decades of experience with the Kentucky coal mining industry; for example, one mine, bidding for a university contract requiring “washed” (implying beneficiated) coal, sprayed the mined coal with water (represented here as samples 5048–5050 in Table 1)).

In this study, we briefly summarize historical data from Kentucky Geological Survey, U.S. Geological Survey, and University of Kentucky Center for Applied Energy Research (CAER) sampling, with the emphasis on the addition of more detailed results from a 2007 sampling of the coal. Geochemistry and mineralogy of the latter samples are discussed in this work. In addition, examples of the inertinite-maceral macrinite in the Gray Hawk were discussed by Hower *et al.* [2], and are further discussed here in light of their implications for our understanding of the role of insects and other arthropods in the development of coal macerals [2,3].

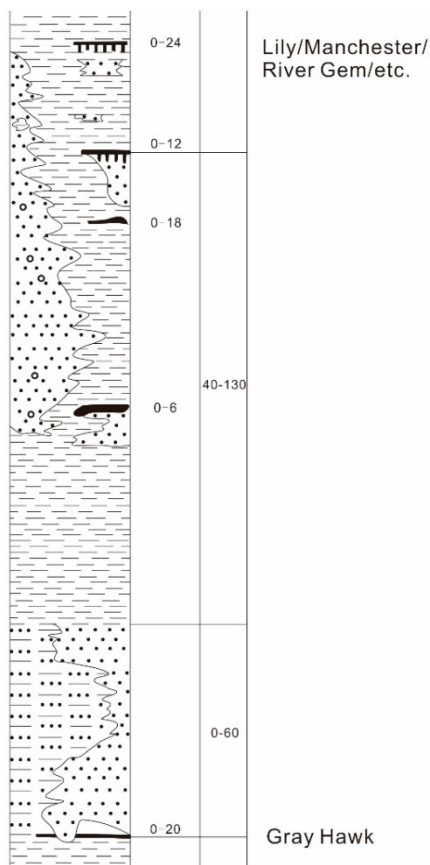


Figure 1. A portion of the Langsettian (Pennsylvanian) geologic section from the Parrot 7.5’ quadrangle [4]. The position of the Gray Hawk coal relative to the Lily and correlative coals is based on the section from the map of the McKee 7.5’ quadrangle [5]. Coal thicknesses are in inches (1 inch = 2.54 cm) and the interval thicknesses are in feet (1 foot = 0.3048 m).

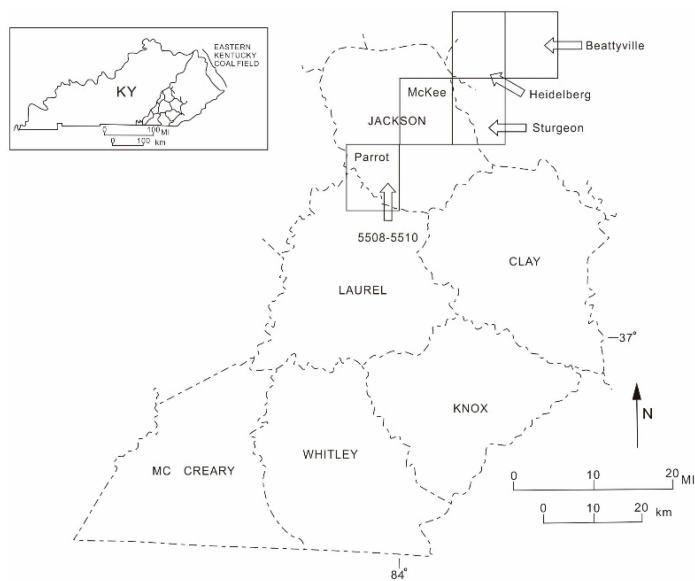


Figure 2. Map of a portion of southeastern Kentucky showing the location of the 7.5’ quadrangles noted on Table 1 and the location of the site of samples 5508–5510 in the Parrot 7.5’ quadrangle.

2. Geological Setting

While broad, basin-wide studies have been made of eastern Kentucky coals [6], no specific studies of the Gray Hawk coal precede this effort. Considering the low-S, and low-ash nature of the coal, perhaps we can draw the low-ash and low-sulfur analogies to the Blue Gem coal [7] and the low-S, low-ash portions of the Blue Gem-correlative Pond Creek coal [8–10]. The implications for the Gray Hawk coal are discussed in Section 4.1, below. Having said that, we observe that Crowder [4] noted occasional black shale above what is probably the Gray Hawk coal.

3. Methods

As noted above, 1980s vintage collections (Table 1) were supplemented by fresh sampling of Gray Hawk coal in a surface mine in the Parrot 7½' quadrangle (samples 5508, 5509 and 5510; 37.319369° N latitude/84.030483° W longitude, Jackson County, Kentucky, USA). The three samples were collected as benches/lithotypes from the full thickness of the mined coal.

Proximate analysis was performed following ASTM (American Society for Testing and Materials) Standards D3173-11 [11], D3175-11 [12] and D3174-11 [13]. Total sulfur and forms of sulfur were determined following ASTM Standards D3177-02 [14] and D2492-02 [15], respectively. Ultimate analysis and heating value determinations were performed based on ASTM Standards D3176-15 [16] and D5865-13 [17], respectively. Oxides of major elements were determined on a Philips PW2404 X-ray Spectrometer (X-ray fluorescence, Philips, Amsterdam, The Netherlands) following procedures outlined by Hower and Bland [8].

Table 1. Location and thickness of 1980s vintage collections.

Sample	Quadrangle	County	N Latitude	W Longitude	Thickness (cm)
5139	McKee	Jackson	37.39278	83.95139	32.00
5028	McKee	Jackson	37.48361	83.89389	40.13
5091	Parrot	Jackson	37.28833	84.07111	32.00
5023	Beattyville	Lee	37.58444	83.70028	35.05
5029	Heidelberg	Lee	37.50972	83.79500	40.64
5048	Sturgeon	Lee	37.49972	83.82389	37.49
5049	Sturgeon	Lee	37.49917	83.82417	42.98
5050	Sturgeon	Lee	37.49889	83.82361	42.67
5185	Sturgeon	Owsley	37.44417	83.78111	45.72
-	Sturgeon	Owsley	37.44432	83.78113	45.01

Inductively coupled plasma mass spectrometry (X series II ICP-MS) (ThermoFisher, Waltham, MA, USA), in pulse counting mode (three points per peak), was used to determine trace elements in the coal samples. For ICP-MS analysis, samples were digested using an UltraClave Microwave High Pressure Reactor (Milestone, Milano, Italy) [18]. Arsenic and Se were determined by ICP-MS using collision cell technology (CCT) in order to avoid disturbance of polyatomic ions [19]. Multi-element standards (Inorganic Ventures: CCS-1, CCS-4, CCS-5 and CCS-6; NIST 2685b and Chinese standard reference GBW 07114) were used for calibration of trace element concentrations. The method detection limit

(MDL) for each of the trace elements, calculated as three times the standard deviation of the average from the blank samples ($n = 10$), is listed in Table 2.

Table 2. Method detection limit (MDL; $\mu\text{g/L}$) of trace elements for ICP-MS analysis.

Trace Elements	MDL						
Li	0.008	Se	0.151	Ba	0.0207	Tm	0.0058
Be	0.0034	Rb	0.3376	La	0.0063	Yb	0.0055
Sc	0.0406	Sr	0.0122	Ce	0.0067	Lu	0.0055
V	0.0131	Y	0.008	Pr	0.007	Hf	0.0121
Cr	0.0215	Zr	0.024	Nd	0.011	Ta	0.0347
Co	0.0067	Nb	0.0455	Sm	0.0067	W	0.1349
Ni	0.1031	Mo	0.1124	Eu	0.0077	Tl	0.0843
Cu	0.0104	Cd	0.0048	Gd	0.003	Pb	0.0143
Zn	0.1542	Sn	0.0486	Tb	0.0064	Bi	0.0362
Ga	0.0015	Sb	0.0152	Dy	0.0091	Th	0.0713
Ge	0.0168	In	0.0024	Ho	0.0052	U	0.001
As	0.0955	Cs	0.0084	Er	0.0009		

Mercury was determined using a Milestone DMA-80 analyzer (Milestone, Milan, Italy). Solid coal samples are directly (without digestion) heated and the evolved Hg is selectively captured as an amalgam and measured by atomic absorption spectrophotometry. The detection limit of Hg is 0.005 ng, the relative standard deviation (RSD) from 11 runs on Hg standard reference is 1.5%, and the linearity of the calibration is in the range 0–1000 ng.

A field emission-SEM (FEI Quanta™ 650 FEG (FEI, Hillsboro, OR, USA), in conjunction with an EDAX energy-dispersive X-ray spectrometer (Genesis Apex 4) (EDAX Inc., Mahwah, NJ, USA), was used to study the modes of occurrence of the minerals, and also to determine the occurrence of selected elements. Samples were carbon-coated using a Quorum Q150T ES sputtering coater (Quorum Technologies Ltd., Lewes, UK), and were then mounted on standard aluminum SEM stubs using sticky conductive carbon tabs. The working distance of the FE-SEM-EDS was 10 mm, beam voltage 20.0 kV, aperture 6, and spot size 5.0. The images were captured via a retractable solid state back-scattered electron detector.

The mineral compositions were determined by X-ray powder diffraction (XRD) (Rigaku, Tokyo, Japan) of low-temperature (oxygen-plasma) ashes of the powdered samples, supplemented by SEM-EDS (FEI, Hillsboro, OR, USA and EDAX Inc., Mahwah, NJ, USA) analysis of the coals in polished section (see below). Low-temperature ashing was carried out using an EMITECH K1050X plasma asher prior to XRD analysis. XRD analysis of the low-temperature ashes was performed on a D/max-2500/PC powder diffractometer with Ni-filtered Cu-K α radiation and a scintillation detector. Each XRD pattern was recorded over a 2θ interval of 2.6° – 70° , with a step size of 0.01° . X-ray diffractograms of the LTAs were subjected to quantitative mineralogical analysis using Siroquant™, commercial interpretation software developed by Taylor [20] based on the principles for diffractogram profiling set out by Rietveld [21]. Further details indicating the use of this technique for coal-related materials are given by Ward *et al.* [22,23] and Ruan and Ward [24].

Petrology was determined on 2.54-cm-diameter epoxy-bound particulate pellets prepared to a final 0.05- μm alumina polish on Leitz Orthoplan microscopes equipped with a 50 \times reflected-light, oil-immersion objective. Vitrinite reflectance was measured with the incoming light polarized at 45 $^\circ$ and the reflected light passing through a 546-nm bandwidth filter on the path to the photomultiplier. The photomultiplier was standardized using glass standards of known reflectance. Maceral identification was based on nomenclature from the International Committee for Coal and Organic Petrology [25,26]. One pellet each of samples 5508, 5509 and 5510 was etched in an acidified saturated solution of potassium permanganate (KMnO_4) in order to show details of vitrinite macerals (procedures after Eble *et al.*) [27].

Palynomorphs were liberated by first oxidizing 2–3 g of < 20 mesh coal with Schulze's Solution (concentrated nitric acid saturated with potassium chlorate). Following oxidation, the samples were digested with 5% potassium hydroxide, repeatedly washed with distilled water, and concentrated with zinc chloride (specific gravity 1.9). Amorphous organic matter (AOM) was removed from the residues using ethylene glycol monoethyl ether (2-ethoxyethanol), ultrasonic vibration, and a short period of centrifugation. Samples were strew-mounted onto 25-mm square cover glasses with polyvinyl alcohol, and fixed to 75 \times 25-mm microscope slides with acrylic resin. Spore and pollen abundances are based on a count of 250 palynomorphs for each sample.

4. Results and Discussion

4.1. Chemistry

The basic coal chemistry and coal petrology data for the previously collected Gray Hawk coal samples are shown in Table 3. With one exception, sample 5028 in the McKee 7 $\frac{1}{2}$ ' quadrangle ($S_t = 3.98\%$), the coal has a low-ash yield and low-S content, mostly varying from 1.68%–5.79% and 0.55%–0.65%, respectively.

Table 4 lists the basic coal chemistry data for the newly-collected Gray Hawk coal samples (samples 5508, 5509 and 5510). These samples exhibit low-ash yields and low-sulfur contents, a characteristic of ombrotrophic peat-forming systems. Such settings have been noted for many coals in the region, including the low-ash, low-S Blue Gem coal [7] and portions of the correlative Pond Creek coal [9,10]. As a consequence of the collapse of the peat dome, leading to a rheotrophic ecosystem, and a brackish or marine incursion, the uppermost coal bench has a medium-sulfur content (1.55%) dominated by pyritic sulfur (0.99%). High-S content has been observed at the top of the coal bed in other eastern Kentucky coals [28–30] as well as coals from other areas (e.g., Chou [31]).

4.2. Petrology

The coal at the Parrott 7 $\frac{1}{2}$ '-quadrangle site is high volatile A bituminous, with a maximum vitrinite reflectance in the 0.8%–0.9% R_{max} range (Table 5). This is generally higher than the rank of the previously studied samples (Table 3). The current study location is further to the southeast and closer to the locus of the high-rank region on the northwest side of the Pine Mountain thrust fault [29,32]. Maceral assemblages are dominated by collotelinite, telinite and vitrodetrinite; fusinite and semifusinite with lesser amounts of micrinite and macrinite; and sporinite with lesser amounts of cutinite (Table 5).

Table 3. As-determined moisture, ash and forms of sulfur; mineral-free-basis maceral groups, and maximum vitrinite reflectance of Gray Hawk coal samples from early 1980s Kentucky Geological Survey and Center for Applied Energy Research collections.

Sample	Proximate Analysis (%)		Sulfur and Forms of Sulfur (%)				HV (MJ/kg)	Maceral (vol %)			R _{o,max}
	M	Ash	S _t	S _{py}	S _{sulf}	S _{org}		V	I	L	
5139	6.00	2.20	0.60	0.14	0.01	0.45	32.05	82.6	11.0	6.4	0.73
5028	4.69	5.79	3.98	2.07	0.01	1.90	30.77	73.1	17.9	9.0	0.73
5091	5.28	1.88	0.65	0.10	0.01	0.54	31.89	79.8	11.5	8.7	0.77
5023	4.11	3.44	0.60	0.08	0.00	0.52	30.87	81.1	11.9	7.0	0.72
5029	5.22	1.68	0.63	0.35	0.01	0.27	31.87	77.3	12.2	10.5	0.81
5048	6.15	1.99	0.55	0.23	0.00	0.32	31.66	79.5	13.2	7.3	0.78
5049	5.47	2.28	0.58	0.30	0.00	0.28	31.70	77.1	11.9	11.0	0.78
5050	5.61	2.74	1.09	0.30	0.01	0.78	31.35	70.4	21.7	7.9	0.75
5185	5.90	1.74	0.64	0.01	0.02	0.61	32.15	78.3	14.9	6.8	0.83

M, Moisture. Ash, ash yield. S_t, total sulfur. S_{py}, pyrite sulfur. S_{sulf}, sulfate sulfur. S_{org}, organic sulfur. HV, heat value. V, vitrinite. I, inertinite. L, liptinite. R_{o,max}, maximum vitrinite reflectance.

Table 4. As-determined proximate and ultimate analyses; forms of sulfur, as-determined heating value of Gray Hawk benches. Unit for moisture, ash yield, volatile matter, fixed carbon, C, H, N, O, and sulfur content, is wt %. Unit for heating value is MJ/kg.

Sample	Bench	Thick (cm)	M	Ash	VM	FC	C	H	N	O	S _t	S _{py}	S _{sulf}	S _{org}	HV
5508	1 of 3 (top)	12.2	2.77	3.04	38.49	55.69	79.63	5.71	1.64	8.43	1.55	0.99	0.02	0.54	32.93
5509	2 of 3	11.8	3.25	1.42	39.03	56.29	80.46	5.76	1.66	9.98	0.72	0.10	0.01	0.61	33.41
5510	3 of 3	8.5	2.76	4.07	40.44	52.73	78.77	5.78	1.61	9.08	0.69	0.08	0.01	0.60	32.84

M, Moisture. Ash, ash yield. VM, volatile matter. S_t, total sulfur. S_{py}, pyrite sulfur. S_{sulf}, sulfate sulfur. S_{org}, organic sulfur. HV, heating value.

Table 5. Petrological compositions and vitrinite maximum reflectance of samples 5508, 5509 and 5510 (%).

Sample	T	CT	VD	CG	T-V	F	SF	Mic	Mac	ID	T-I	Sp	Cut	Res	LipD	T-L	R _{o,max}
5508	12.6	42.9	6.7	0.8	63.0	14.0	8.1	2.6	1.4	0.4	26.5	7.7	2.6	0.0	0.2	10.5	0.89
5509	14.0	56.5	6.6	0.6	77.8	2.2	4.8	1.6	1.6	0.2	10.4	10.6	1.2	0.0	0.0	11.8	0.86
5510	12.8	38.5	12.2	3.2	66.7	9.8	5.0	1.2	0.8	0.2	17.0	14.2	1.0	0.4	0.6	16.2	0.82

T, telinite; CT, collotelinite; VD, vitrodetrinite; CG, corpogelinite; T-V, total vitrinite; F, fusinite; SF, semifusinite; Mic, micrinite; Mac, macrinite; ID, inertodetrinite; T-I, total inertinite; Sp, sporinite; Cut, cutinite; Res, resinite; LipD, liptodetrinite; T-L, total liptinite; R_{o,max}, random vitrinite maximum reflectance.

Cutinite was noted to occur in association with possible epiphyllous fungi (funginite) (Figure 3). While such forms are not well known before the Cretaceous, Taylor *et al.* [33] and Burlington [34] did note epiphyllous fungi in association with Stephanian pteridosperms. *Verrucosporites*, not observed in the palynomorph counts, was noted in the bottom bench during petrography studies (sample 5510) (Figure 4A,B). The megaspore *Triletes globosus* (Figure 4C,D) would have been excluded from the miospore slides due to the screening step during processing. Thin vitrinertoliptite canal bands were noted in the bottom bench (sample 5510) (Figure 5). Without oriented block samples, we cannot establish the location of the canal within the bench.

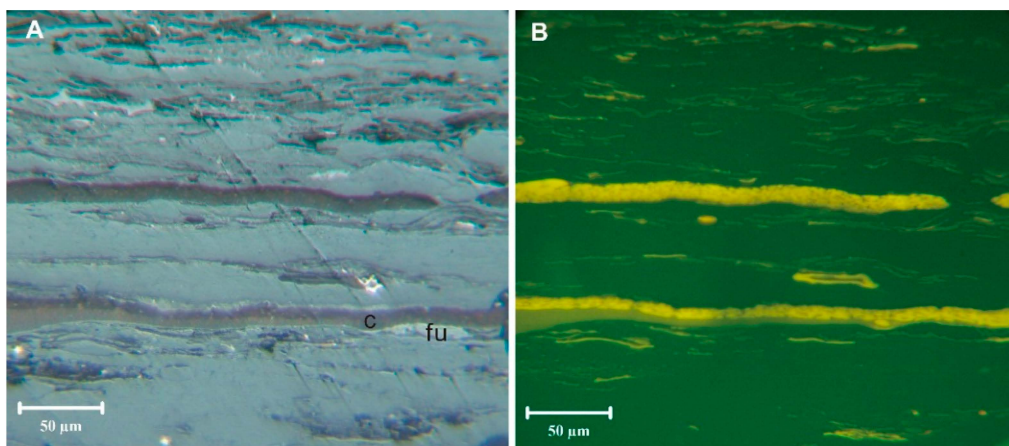


Figure 3. Cutinite in sample 5510. Epiphyllous fungi (fu) growing on cutinite (c). (A) Reflected light, oil immersion; (B) Blue-light.

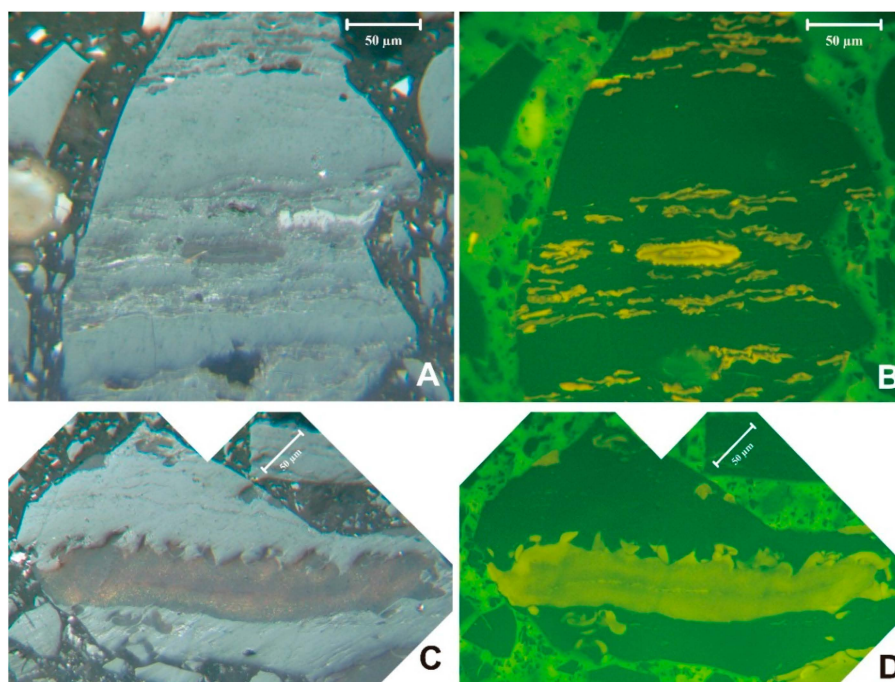


Figure 4. Sporinite in sample 5510. (A) and (B) *Verrucosporites* (larger ornamented spore in lower center) with smaller *Lycospora* in mixed maceral matrix. (C) and (D) megaspore, probably *Triletes globosus*. (A) and (C) reflected light, oil immersion. (B) and (D) blue-light.

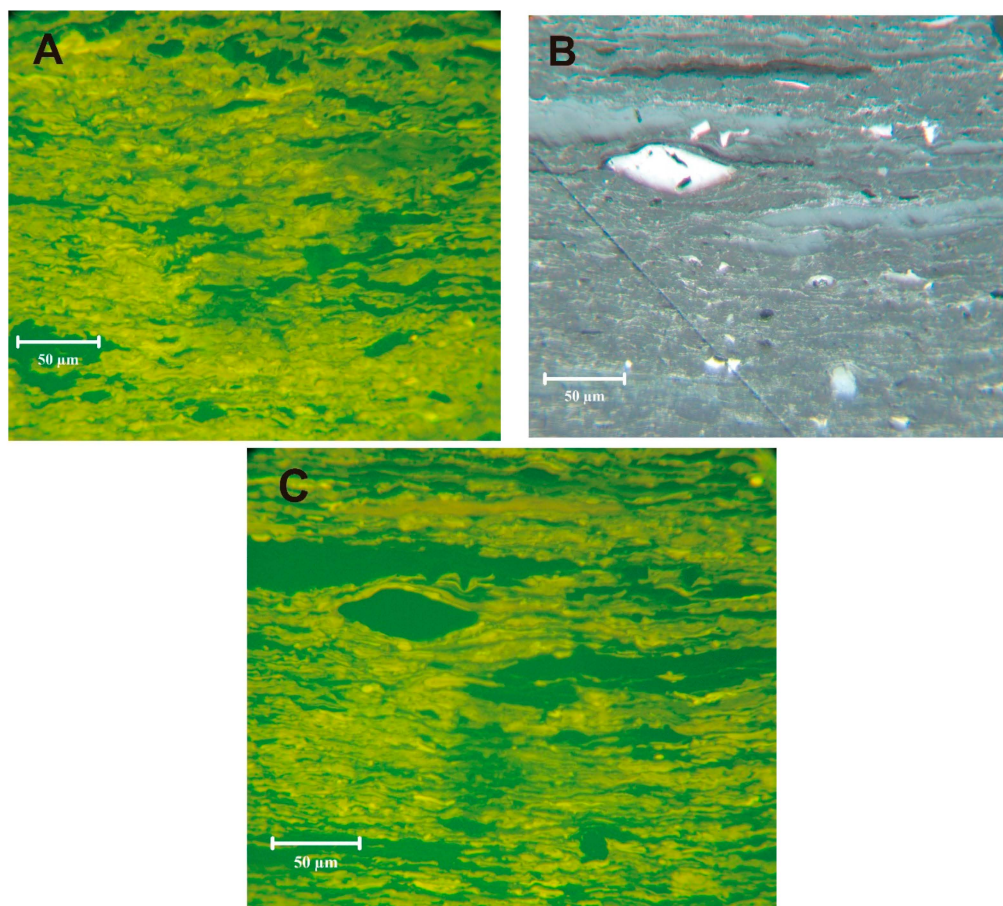


Figure 5. Cannel in sample 5510. (A) canal; (B) and (C) canal with vitrinite bands and inertinite fragments; (A) and (C) blue-light; (B) reflected light, oil immersion.

Fusinite and semifusinite occur as both primary, direct fire-derived varieties and forms which were degraded and then charred. The primary, fire-derived origin of fusinite has long been established [35,36], with more recent advocacy on the part of Scott and his co-workers, among others [37–48]. Certain inertinite macerals with a fusinite and semifusinite reflectance took a more convoluted path, undergoing varying degrees of degradation prior to charring [49,50], and likely charring at a range of temperatures [47,48,51].

A variety of primary fusinite (such as in Figure 6A,B) and fusinite- and semifusinite-levels of reflectances occur in inertinites subjected to charring after degradation (Figure 6A,C,D). Both the fusinite- and semifusinite-reflectance macerals in Figure 6C and, in particular, the semifusinite- reflectance maceral in Figure 6D have swollen cell walls typically associated with fungal or bacterial degradation [52,53].

Macrinite, at least in part, is a product of the ingestion and excretion of woody material with possible (or likely) successive cycles of fungal and bacterial colonization and/or coprophagous recycling [49,50,54–57]. In part, the complexity of macrinite structure, particularly the inclusion of fusinite and liptinite within the macrinite, underwent significant changes from the Devonian [58–60] to the Pennsylvanian [4,61,62], the Cretaceous and later [5,49,54,63]. Much of this was due to the expansion and evolution of insects and other arthropods. Raymond *et al.* [64] note that, while the three extant digestive schemes employed by modern detritivores (external rumen, facultative mutualism

and symbiosis) existed in the Pennsylvanian, the faunal participants were different. This difference is exemplified in the difficulty of assigning fossil arthropod coprolites to their producers [58,59,65–68]. Further, the rate of fungal, bacterial, and detritivore decomposition was slower in the Pennsylvanian compared to younger settings [64]. In the latter context, the inclusions in the macrinite on the right side of Figure 7A demonstrate that non-discriminating feeding activity was part of the Langsettian ecosystem. Much more common in Pennsylvanian coals is relatively inclusion-free macrinite (Figure 7A,B,F,G and the macrinite across the center of Figure 7H). Fecal pellet-derived macrinite (Figure 7C–E,H), common in younger coals [49], was previously noted in a survey of Pennsylvanian macrinite [4]. This should not be a surprise; if something was ingesting the wood, excretion would be a necessary function. The Cretaceous forms are dominated by individual pellets while the Gray Hawk forms appear to be merged into larger masses, consistent with Type 1 coprolites as defined by Taylor and Scott [62], albeit with some indication that the origin was from individual pellets. The compaction and merger may be a function of the moisture content of the original pellets, the vegetal composition of the diet and the subsequent fecal pellet, the wet vs. dry nature of the depositional (and subsequent) environment, or a combination of all of the above plus coalification and other unaccounted for influences. Given the small size of the individual pellets forming the coprolite masses, collembola or perhaps an extinct group of herbivores or detritivores, may have produced them [49].

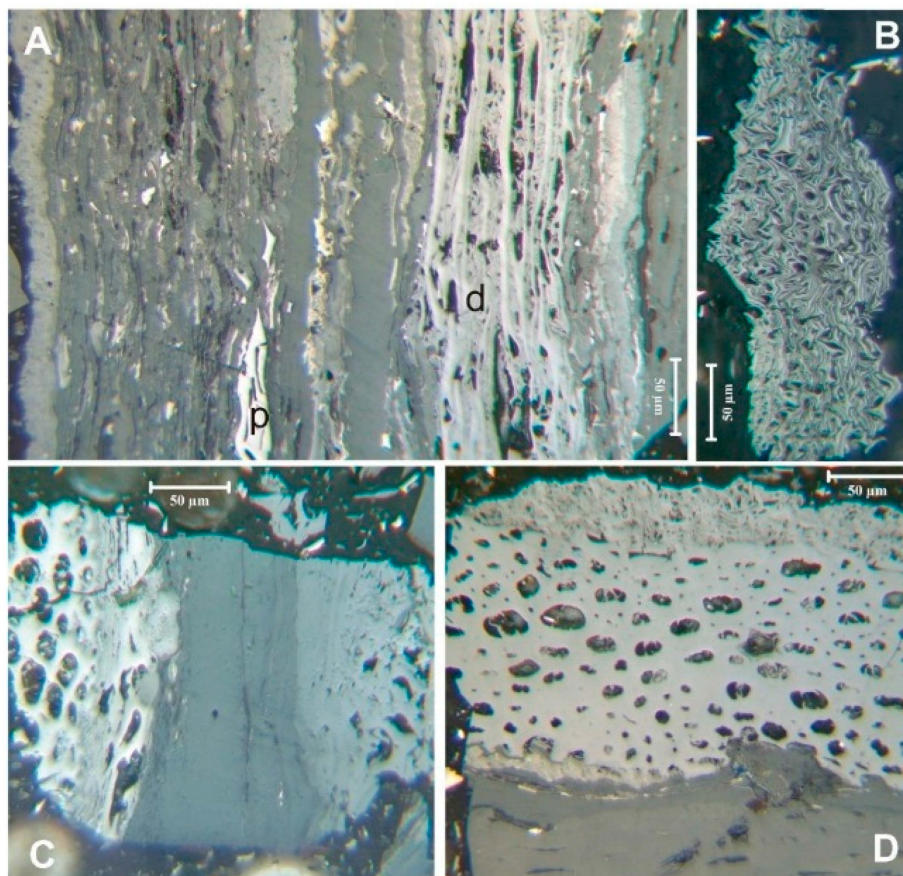


Figure 6. Fusinite and semifusinite in the coal. (A) mix of primary (p) and degraded (d) fusinite and semifusinite; (B) primary fusinite; (C) degraded fusinite and semifusinite; (D) degraded semifusinite. Reflected light, oil immersion.

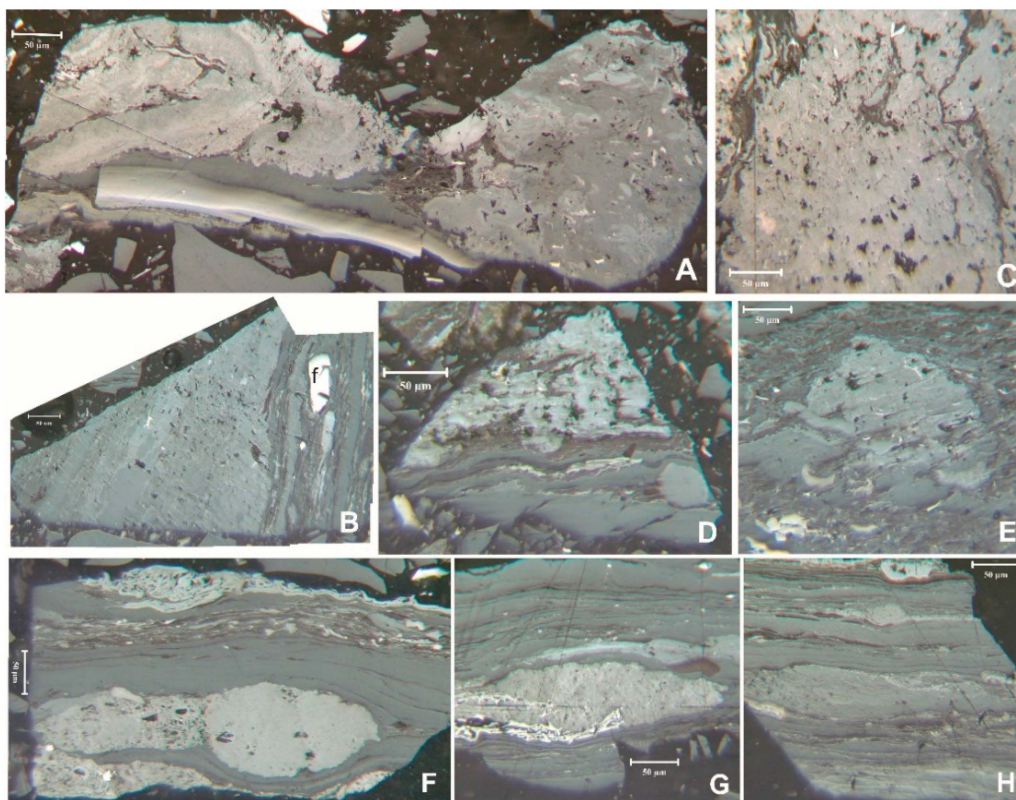


Figure 7. Macrinite in the coal. (A) macrinite with inertodetrinite inclusions on right; macrinite on left may have replaced sporinite, as noted in the Hower *et al.* [4] publication of the image, or it may just have a shape coincident with sporinite; note that Hower and Ruppert [55] showed an example of funginite replacing a megaspore in a Pennsylvanian coal; (B) assemblage of macrinite (ma), semifusinite (sf), and fusinite (f); (C) agglomerated rounded macrinite reminiscent of fecal pellet macrinite seen in younger coals [49]; from Hower *et al.* [4]; (D) agglomerated rounded macrinite reminiscent of fecal pellet macrinite; (E) macrinite with inertodetrinite inclusions but also with agglomerated rounded macrinite reminiscent of fecal pellet macrinite; (F) macrinite (ma) with semifusinite (sf); (G) macrinite (ma) with fusinite; (H) fecal pellet macrinite (fp), Reflected light, oil immersion; (A–E) sample 5510; (F) sample 5028; (G) and (H) sample 5023. Scale bar: 50 µm.

Vitrinite counts were made on the unetched pellets; the observations here are based on the details revealed in the etching process. Based on the etched pellets the telinite and collotelinite have superficial similarities in the unetched portion of Figure 8A. Etching emphasizes the fundamental differences in maceral structure, with the telinite band shown to largely consist of cell walls and the collotelinite band showing a more uniform structure. Telinite is also seen in Figure 8B and in the lower half of Figure 8C. The upper half of the Figure 8C vitrinite particle consists of corpogelinite cell fillings surrounded by telinite cell walls. Similarly, that in Figure 8D has bands of corpogelinite with thin cell walls. The latter bands are separated by *ca.* 10-µm bands, probably originating from detrovitrinite.

Petrographically, the relatively high vitrinite contents, especially telovitrinite which peaks in the middle bench, are likely a function of the same wet conditions that promoted arborescent lycopods,

pteridospermalean and cordaitalean gymnosperms, as well as the relatively slower rates of decomposition present in the Pennsylvanian coal bed. A direct correspondence between high vitrinite contents and high percentages of arborescent lycopod spores, especially *Lycospora*, is a common feature in many Early and Middle Pennsylvanian coal beds in the Appalachian and Eastern Interior, USA basins [69–74]. The decrease in fusinite + semifusinite from the bottom bench to the middle bench, followed by a large increase to the top bench, is a further indication of the cycle of relative wet and dry conditions in the Gray Hawk coal.

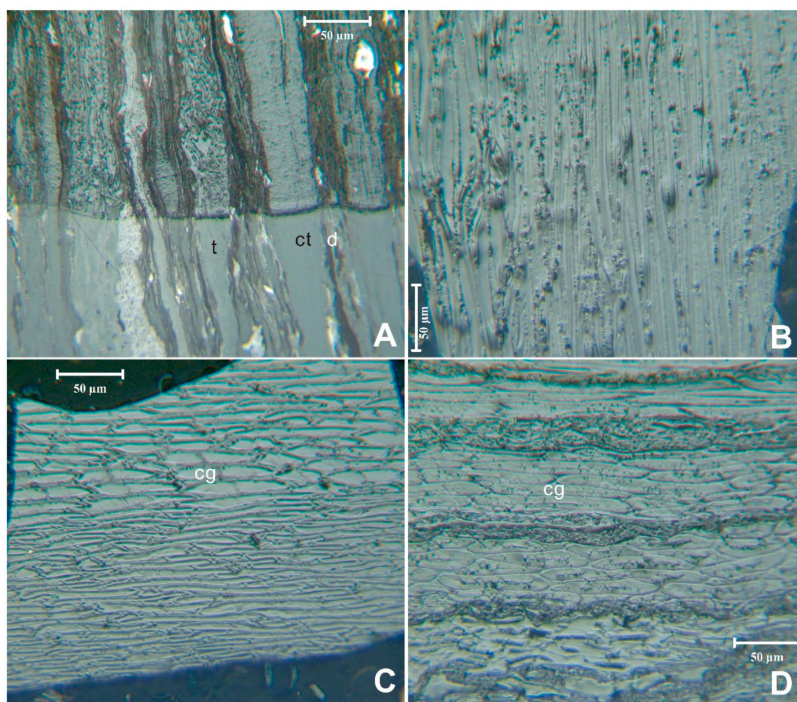


Figure 8. Vitrinite in the coal. (A) etched vitrinite, inertinite, and liptinite showing contrast between telinite (t), collotelinite (ct), and detrovitrinite (d) bands; (B) etched telinite; (C) etched corpogelinite (cg) cell filling with telinite cell walls; (D) etched corpogelinite (cg) cell filling with telinite cell walls, Reflected light, oil immersion; (A) sample 5509; (B) sample 5510; (C) and (D) 5509.

4.3. Palynology

Palynomorph data is reported as percentages of the total count in Table 6, according to parent plant affinity. Palynomorph/parent plant affinities are based on excellent summaries by [75–77]. Forms identified in addition to those observed in the point counts are marked with an X in Table 6.

The occurrence of a few, stratigraphically constrained, spore taxa indicate a late Early Pennsylvanian (late Langsetian) age for the Gray Hawk coal bed. These taxa include *Schulzospora rara*, *Radiizonates aligerans*, *R. striatus*, *Secarisporites remotus*, *Endosporites globifomis*, *Laevigatosporites* spp. and *Granasporites medius* [74]. The Gray Hawk coal palynoflora is strongly dominated by *Lycospora* spp. (>85% in all three samples), which is typical of coal beds in this stratigraphic interval. Indeed, many, if not most, Early Pennsylvanian coal beds in the Appalachian Basin are dominated by *Lycospora* spp., which is the dispersed spore genus of several of the large lycopsid trees (e.g., *Lepidodendron*,

Lepidophloios) that were important elements of Early Pennsylvanian mire floras [71–74,78]. *Lycospora pellucida* and *L. pusilla* are abundant in all three benches (Table 6). *Lycospora granulata* is relatively abundant in the bottom two benches, exceeding the concentration of *L. pusilla* in the bottom bench, but undergoes a precipitous drop in concentration to the top bench, sample 5508. Small ferns, particularly represented by *Granulatisporites parvus*, and calamites (*Calamospora breviradiata*) in the bottom bench, are present in lesser abundance than the lycosids. Cordaites, primarily *Florinites* spp., occur in all three benches, but reach significant abundances in the bottom and middle benches. Common palynomorph taxa recovered from the Gray Hawk coal bed are shown in Figure 9.

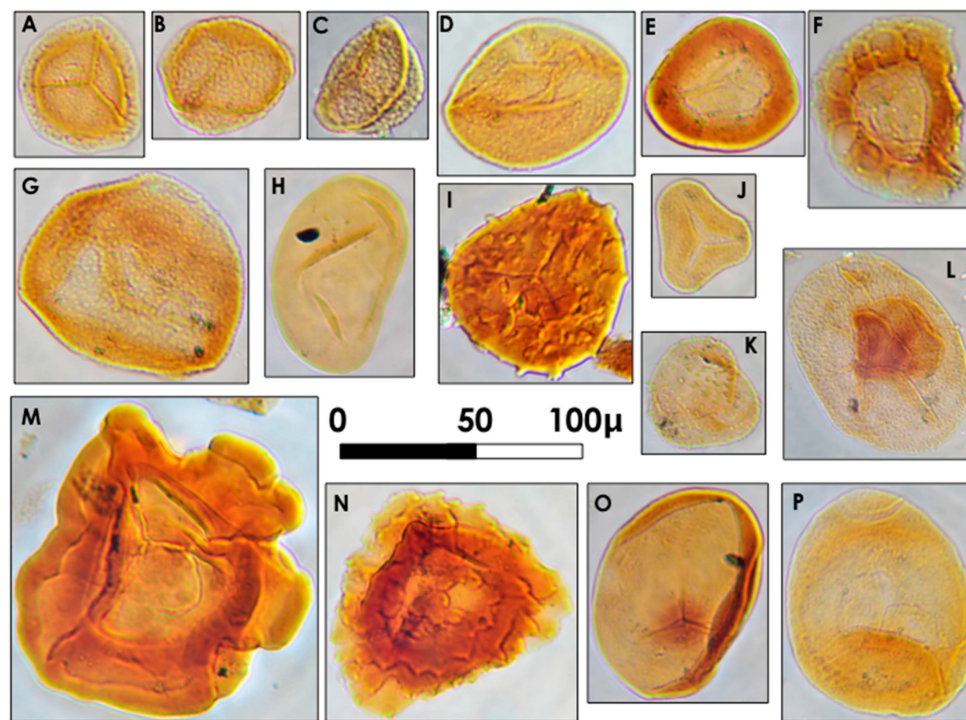


Figure 9. Common palynomorphs in the Gray Hawk coal bed. (A) *Lycospora pellucida*; (B) *Lycospora pusilla*; (C) *Lycospora granulata*; (D) *Granasporites medius*; (E) *Densosporites annulatus*; (F) *Radiizonates aligerans*; (G) *Crassispora kosankei*; (H) *Laevigatosporites minor*; (I) *Camptotriletes bucculentus*; (J) *Granulatisporites adnatoides*; (K) *Pilosporites triquetrus*; (L) *Florinites similis*; (M) *Reticulatisporites reticulatus*; (N) *Cristatisporites connexus*; (O) *Calamospora breviradiata*; (P) *Schulzospora rara*. All images were collected using Nomarski interference contrast illumination (DIC).

Table 6. Palynology of Gray Hawk benches. Note: X indicates that the palynomorph was observed to occur in trace amounts.

Sample	5508	5509	5510	Sample	5508	5509	5510	Sample	5508	5509	5510
<i>Lycospora pellucida</i>	46.8	37.2	41.2	<i>Granulatisporites parvus</i>	5.6	2.4	2.4	<i>Schulzospora rara</i>			1.6
<i>L. pusilla</i>	32.8	30.4	22.4	<i>G. adnatoides</i>	X	X	X	Total Seed Ferns	0.0	1.6	0.0
<i>L. granulata</i>	3.2	22.0	25.6	<i>G. piroformis</i>	X	X	X	<i>Calamospora breviradiata</i>	0.8	X	0.4
<i>L. orbicula</i>	X	X	X	<i>G. granulatus</i>	X			<i>C. microrugosa</i>	X	X	
<i>L. micropapillata</i>	3.2	0.4	3.2	<i>Cyclogranisporites microgranus</i>	X			<i>C. pallida</i>	X		X
<i>L. rotunda</i>	X	X	X	<i>C. minutus</i>		X		<i>C. parva</i>		X	
<i>L. torquifer</i>	X	X		<i>Lophotriletes microsaeetus</i>	0.8	0.4		<i>Laevigatosporites minor</i>	0.4	0.8	2.0
<i>Granasporites medius</i>	3.2	3.2	X	<i>L. commissuralis</i>	X	X	X	<i>L. vulgaris</i>			0.4
<i>Crassispora kosankei</i>	X	X	X	<i>L. granoornatus</i>		X		<i>Reticulatisporites reticulatus</i>		X	0.4
Total Lycopsid Trees	89.2	93.2	92.4	<i>Leiotriletes subadnatoides</i>	1.2	X	X	<i>R. muricatus</i>	X	X	
<i>Densosporites annulatus</i>	X	X	0.4	<i>L. adnatus</i>	X	X		Total Calamites	1.2	0.8	3.2
<i>D. triangularis</i>	X			<i>L. pridyii</i>	X			<i>Florinites florini</i>	0.8	0.4	X
<i>D. sphaerotriangularis</i>	0.8	0.4	X	<i>Pilosisporites triquetrus</i>	X	X		<i>F. mediapudens</i>	X	X	
<i>Cristatisporites indignabundus</i>	X	X	X	<i>P. aculeolatus</i>	X		X	<i>F. similis</i>	X		
<i>C. connexus</i>	X	X		<i>Savitrissporites majus</i>	X	X		<i>F. milotti</i>			X
<i>Cingulizonates loricatus</i>	X	X		<i>Camptotriletes bucculentus</i>	X	X	X	Total Cordaites	0.8	0.4	0.0
<i>Radiizonates aligerans</i>	X	X	X	<i>C. corrugatus</i>	X	X		<i>Potonieisporites elegans</i>			X
<i>R. striatus</i>		X		<i>Verrucosisporites verrucosus</i>	X	X	X	Total Conifers	0.0	0.0	0.0
<i>Cirratriradites saturni</i>	X		X	<i>V. donarii</i>	X	X		<i>Ahrensiaeporites guerickei</i>	X		
<i>Endosporites globiformis</i>	X	X	X	<i>Convolutispora florida</i>	X	X		<i>Secarisporites remotus</i>	X	X	
<i>E. ornatus</i>		X		<i>Reticulitriletes reticulocingulum</i>		X		<i>Reinschospora magnifica</i>	X		
<i>Spencerisporites radiatus</i>	X	X	X	<i>R. falsus</i>	X			<i>Dictyotriletes bireticulatus</i>	X	X	X
Total Small Lycopsids	0.8	0.4	0.4	<i>Microreticulatisporites concavus</i>		0.8	0.4	<i>Grumosisporites varireticulatus</i>	X	X	
<i>Punctatisporites minutus</i>	0.4	X	1.2	<i>Raistrickia abdita</i>	X	X		Total Unknown Affinity	0.0	0.0	0.0
<i>Laevigatosporites minimus</i>		X		<i>R. saetosa</i>			X				
Total Tree Ferns	0.4	0.0	1.2	<i>Apiculatisporis variocorneus</i>	X	X	X				
				<i>Apiculatasporites spinulistratus</i>	X	X					
				<i>Punctatisporites punctatus</i>	X						
				<i>P. aerarius</i>	X	X					
				Total Small Ferns	7.6	3.6	2.8				

Abundant *Lycospora* spp. spores indicate that arborescent lycopsids, notably *Lepidophloios* and *Lepidodendron*, were contributors to the peat that formed the Gray Hawk coal bed. The proportion of *Granasporites medius* in the samples indicates that *Diaphorodendron* and/or *Synchysidendron*, was also present, though likely in proportionally fewer numbers than *Lepidophloios* or *Lepidodendron*. Mire-centered lycopsids had developed reproductive and vegetative strategies for growth and development in very wet areas. The megasporangium of *Lepidophloios* (*Lepidocarpon*) and *Lepidodendron* (*Achlamydocarpon*) were both boat-shaped, facilitating dispersal in areas of standing water. Lycopsid root systems (*Stigmaria*) radiated laterally from the base of the plant, rather than downward, to provide stability. This is a common feature of many modern tree-size plants growing in wet, soft substrates. Furthermore, the rootlets emanating from *Stigmarian* axes were very slender in design, and would have been incapacitated by firm substrates [78].

Other plant groups, ferns, seed ferns, calamites and cordaites, are represented by minor quantities of palynomorphs in the Gray Hawk coal bed. The same supersaturated substrates that would have favored the proliferation of arborescent lycopods may have also favored pteridospermatophytean and cordaitalean gymnospermous trees [79]. Both taxa produced fewer palynomorphs than the lycopsid taxa, and may have been, at least to a degree, arthropod pollinated [68]. The presence of coprolitic macrinite in the samples supports the supposition that saprophytic and/or grazing arthropods occurred in the mire ecosystem; these and others may have served as pollinators for the early gymnosperms.

4.4. Geochemistry

Table 7 lists the percentages of major-element oxides and concentrations of trace elements in the newly-collected samples (5508, 5509 and 5510). Due to the low ash yields, the major-element oxide contents are very low relative to those in coals of other areas (e.g., Dai *et al.* [80]). Iron content is highest in the upper bench (48.24 wt % Fe_2O_3) falling to 5.70 wt % in the lowermost bench with concomitant increases in silica, alumina and titanium. Calcium concentration is highest in the middle bench.

Compared to average values for world hard coals reported by Ketris and Yudovich [81], Ge and As are slightly enriched in the coal with concentration coefficients between 2-5 (CC, ratio of trace element concentration in studied samples vs. averages for world hard coals); however, the concentrations of other trace elements are either close to or much lower than world averages (Figure 10).

With the exception of As (28.04 $\mu\text{g/g}$), most elements of environmental concern in the coal are low in concentrations, such as Be (2.53 $\mu\text{g/g}$ on average for the three benches), Cr (5.65 $\mu\text{g/g}$), As (28.04 $\mu\text{g/g}$), Se (2.02 $\mu\text{g/g}$), Cd (0.05 $\mu\text{g/g}$), Mo (0.54 $\mu\text{g/g}$), Hg (174 ng/g), Tl (0.23 $\mu\text{g/g}$), Pb (12.34 $\mu\text{g/g}$) and U (0.31 $\mu\text{g/g}$). Arsenic and Hg are also enriched in the top bench (sample 5508). This is also the bench with the highest pyritic sulfur content (Table 1), and, as discussed more fully below, the highest proportion of pyrite both within the LTA and the whole-coal material. Such an occurrence suggests an association with the sulfide minerals, in accordance with the observations of many other authors [82–90].

A number of elements (Li, Be, Sc, V, Cr, Co, Ni, Cu, Zn, Ga, Ge, Se, Zr, Nb, Th, U and REY) are relatively enriched in the lower bench. Enrichment of Zr + TiO_2 in the basal lithotype of eastern Kentucky coals has been noted in other studies, for example Hower and Bland [8]. Considering the known association of U and Th with zircons, more abundant zircon in the basal bench may explain the greater abundance of U and Th in the coal. The lowermost bench (sample 5510) has the highest ash yield

(Table 4) and also (as described below) the highest proportion of illite and illite/smectite among the clay minerals. Vanadium and Cr are known to be associated with clay minerals [91,92], and in some cases with organic matter [93]. These two elements in the present study are thus probably associated with the more abundant clay minerals, especially illite and illite/smectite, in the lower bench sample.

Germanium, enriched in both the top and, in particular, the bottom bench, has been found to be enriched in the same position in many other coals [94,95]. The element is generally associated with organic matter [96], and its enrichment is usually attributed to the leaching of granite by hydrothermal solutions and the Ge-rich solutions discharged into the peat swamp [80,96]. Copper and Zn are associated with traces of chalcopyrite and sphalerite, respectively, as described more fully below.

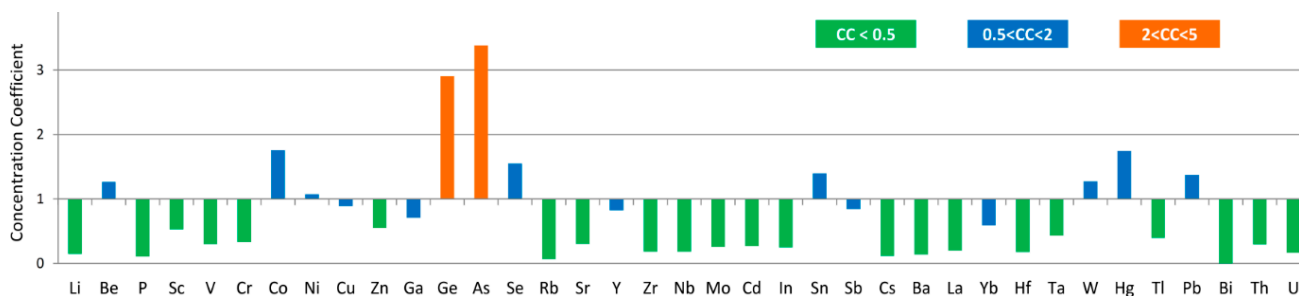


Figure 10. Concentration coefficients (CC) of trace elements in the Gray Hawk coals, normalized by average trace element concentrations in world hard coals [81].

The $\text{Al}_2\text{O}_3/\text{TiO}_2$ ratio is a useful provenance indicator for sedimentary rocks [97] and sediments associated with coal deposits [63]. Typical $\text{Al}_2\text{O}_3/\text{TiO}_2$ ratios are 3-8, 8-21, and 21-70 for sediments derived from mafic, intermediate, and felsic igneous rocks, respectively [97]. The three benches of the Gray Hawk coals have $\text{Al}_2\text{O}_3/\text{TiO}_2$ ratios of 16.8 (sample 5508), 22.1 (sample 5509), and 17.7 (sample 5510), indicating a sediment-source region with intermediate and felsic compositions; this is also supported by the relationship of $\text{Cr}/\text{Th}-\text{Sc}/\text{Th}$ (Figure 11). However, the relationship of Co/Th vs. La/Sc plot (Figure 11) indicates a minor input of intermediate-mafic materials.

Although the rare metals (Ga; rare earth elements and yttrium, REY or REE if Y is not included) in the coal samples are relatively low in concentration compared to world averages, they are, as along with Ge, highly enriched in the coal ashes (Table 8). Based on the cut-off grade (higher than $1000 \mu\text{g}/\text{g}$) for beneficial recovery of REY from coal combustion products as proposed by Seredin and Dai [98], the Gray Hawk coals have great potential for industrial use. The $\text{REY}_{\text{def, rel}}-\text{Coutl}$ graph, which was proposed by Seredin and Dai [98] to evaluate of REY-rich ashes as raw materials (Figure 12), where the X-axis is the outlook coefficient (Coutl, ratio of the relative amount of critical REY metals in the REY sum to the relative amount of excessive REY) and the Y-axis is the percentage of critical elements in total REY ($\text{REY}_{\text{def, rel}}$, %), shows that the REY in the three coal bench samples (ash basis) fall in Area III or between Areas II (promising) and III (highly promising).

Table 7. Concentrations of major-element oxides and trace elements in the samples 5508, 5509 and 5510, as well as their comparison with averages for world hard coals (Unit for loss-on-ignition and major-element oxides is %; Unit for trace elements is $\mu\text{g/g}$ and for Hg is ng/g).

Sample	SiO ₂	TiO ₂	Al ₂ O ₃	Fe ₂ O ₃	MgO	CaO	Na ₂ O	K ₂ O	P ₂ O ₅	SO ₃	LOI	Li	Be	Cl	Sc	V	Cr	Co	Ni	Cu
5508	27.97	0.92	15.4	47.64	0.54	2.91	0.37	0.98	0.23	2.08	96.96	1.39	1.83	2608	0.92	4.61	3.31	4.22	9.56	6.44
5509	36.16	1.35	29.85	18.18	0.88	6.43	1.08	0.78	0.33	3.91	98.58	1.22	1.76	3571	0.49	3.63	2.51	9.73	9.32	11.18
5510	52.98	1.74	30.9	5.7	0.78	2.36	0.88	2.41	0.18	1.31	95.93	4.35	4.60	2743	5.49	20.54	13.36	20.71	43.1	29.74
Average	37.48	1.29	24.70	25.97	0.73	4.04	0.76	1.28	0.25	2.54	97.16	2.1	2.53	2993	1.96	8.42	5.65	10.53	18.24	14.25
World	nd	nd	nd	nd	nd	nd	nd	nd	nd	nd	nd	14	2	340	3.7	28	17	6	17	16
Sample	Zn	Ga	Ge	As	Se	Rb	Sr	Y	Zr	Nb	Mo	Cd	In	Sn	Sb	Cs	Ba	La	Ce	Pr
5508	7.66	3.12	1.72	71.11	2.12	0.83	30.47	4.9	4.81	0.47	0.8	0.03	0.01	1.21	0.38	0.09	24.69	1.87	3.66	0.54
5509	8.08	1.98	0.24	1.93	1.07	bdl	28.45	4.62	3.83	0.3	0.5	0.01	0.01	3.42	0.06	0.02	14.46	1.7	4.17	0.62
5510	36.73	9.03	23.83	2.48	3.18	3.44	33.44	13.03	13.02	1.72	0.24	0.15	0.01	0.99	2.6	0.33	25.28	3.41	7.21	1.04
Average	15.42	4.25	6.97	28.04	2.02	1.21	30.51	6.92	6.6	0.74	0.54	0.05	0.01	1.95	0.84	0.13	21.13	2.21	4.77	0.7
World	28	6	2.4	8.3	1.3	18	100	8.4	36	4	2.1	0.2	0.04	1.4	1	1.1	150	11	23	3.4
Sample	Nd	Sm	Eu	Gd	Tb	Dy	Ho	Er	Tm	Yb	Lu	Hf	Ta	W	Hg	Tl	Pb	Bi	Th	U
5508	2.39	0.56	0.14	0.64	0.12	0.68	0.15	0.47	0.06	0.35	0.06	0.15	0.06	1.68	425	0.61	15.67	bdl	0.76	0.16
5509	2.86	0.7	0.15	0.75	0.11	0.65	0.12	0.37	0.04	0.27	0.03	0.1	bdl	1.3	22	bdl	3.91	bdl	0.41	0.11
5510	4.74	1.25	0.32	1.54	0.31	2.23	0.46	1.47	0.19	1.39	0.18	0.46	0.41	0.6	26	bdl	19.28	bdl	1.95	0.82
Average	3.18	0.79	0.19	0.92	0.17	1.07	0.22	0.7	0.09	0.59	0.08	0.21	0.13	1.26	174	0.23	12.34	0	0.94	0.31
World	12	2.2	0.43	2.7	0.31	2.1	0.57	1	0.3	1	0.2	1.2	0.3	0.99	100	0.58	9	1.1	3.2	1.9

nd, no data; bdl; below detection limit.

Table 8. Rare metals (Ga, Ge and REY) in the ash of Gray Hawk coal ($\mu\text{g/g}$).

Sample	Ga	Ge	La	Ce	Pr	Nd	Sm	Eu	Gd	Tb	Dy	Y	Ho	Er	Tm	Yb	Lu	REY	REO
5508	99.8	54.9	59.6	117	17.2	76.3	17.8	4.31	20.4	3.77	21.9	157	4.89	15.0	1.88	11.1	1.76	529	635
5509	135	16.1	116	284	42.1	195	47.4	10.1	51.2	7.45	44.0	315	8.33	24.9	2.64	18.6	2.37	1168	1402
5510	215	569	81.4	172.11	24.9	113	29.7	7.70	36.8	7.34	53.2	311	11.0	35.1	4.50	33.2	4.26	925	1110
Average	143	175	85.77	192	28.26	129	31.7	7.30	35.9	6.04	38.1	254	7.75	23.8	2.84	19.6	2.64	865	1038

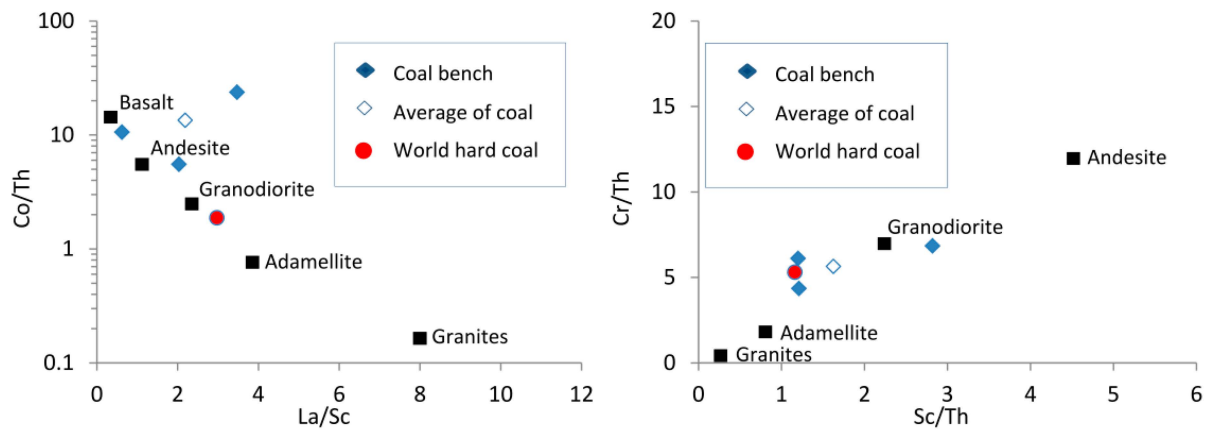


Figure 11. Relationship of Co/Th against La/Sc [99] and Cr/Th against Sc/Th [100] for the Gray Hawk coal samples. Data of different igneous rocks are from Condie [99].

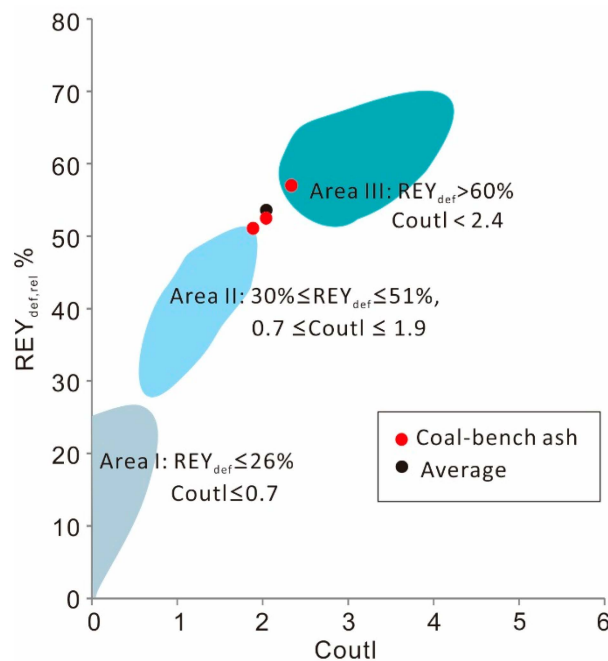


Figure 12. The $REY_{def,rel}$ - $Coutl$ plot for Gray Hawk coal ashes. Area I, unpromising, Area II, promising, and Area III, highly promising.

The classification of REY used in the present study is based on Seredin and Dai [98] and includes light (LREY: La, Ce, Pr, Nd and Sm), medium (MREY: Eu, Gd, Tb, Dy and Y), and heavy (HREY: Ho, Er, Tm, Yb and Lu) REY. Accordingly, in comparison with the upper continental crust (UCC) [101], three enrichment types are identified: L-type (light-REY; $La_N/Lu_N > 1$), M-type (medium-REY; $La_N/Sm_N < 1$, $Gd_N/Lu_N > 1$), and H-type (heavy-REY; $La_N/Lu_N < 1$) [98]. The REY in samples 5508 and 5509, however, have similar distribution patterns; both are weakly fractionated (Figure 13) but are slightly enriched in medium- and heavy-REY. Sample 5510 is distinctively characterized by a heavy-REY enrichment type (Figure 13). The three samples do not show anomalies of Eu, Ce and Y (Figure 13). However, the REE distribution patterns of the coal samples present in this study would have been expected to have a light-REY enrichment type because the sediment-source region is mainly of felsic to intermediate composition. The REY in the present coal samples may have been subjected to acid natural

waters or epithermal solutions, which can lead to the medium-REY [98,102] and heavy-REY [98,103] enrichment types, respectively.

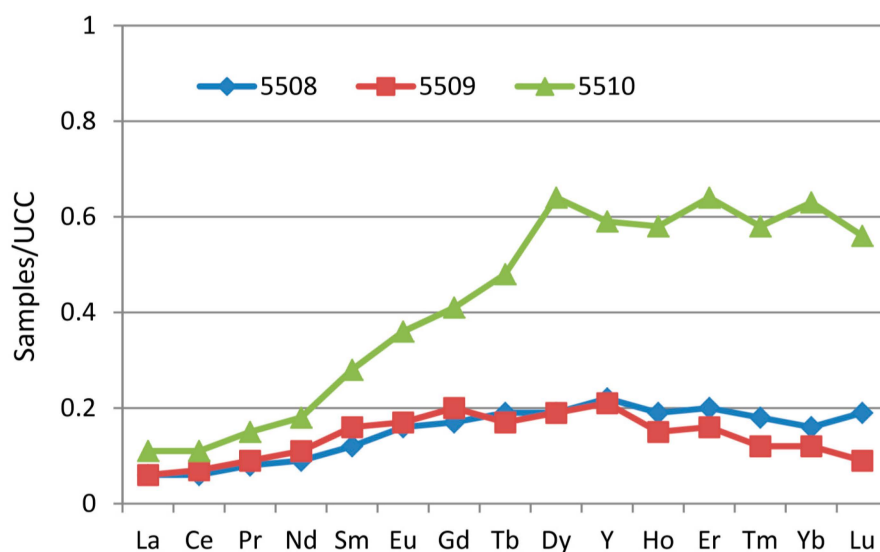


Figure 13. Distribution patterns of REY in the Gray Hawk coals. REY are normalized by Upper Continental Crust [101].

The concentration of Ge in the Gray Hawk coal ash is 18-times higher than that in the world hard coal ashes reported by Ketris and Yudovich [81]. For comparison, the Ge concentration in the ashes of coal-hosted Ge ore deposits including Wulantuga, Lincang, and Spetzugli, are 2820, 3902 and 4906 $\mu\text{g/g}$, respectively [104]. Germanium is currently being industrially extracted as a raw material from these three Ge-bearing coal deposits. Gallium concentrations in the coal-ash samples are 103, 139 and 222 $\mu\text{g/g}$, respectively, much higher than the average value for world hard coal ash (36 $\mu\text{g/g}$) [81]. The average concentration of Ga in fly ash derived from the coal-hosted Al-Ga ore deposit in Jungar, Inner Mongolia, China, is 92 $\mu\text{g/g}$ [105].

4.5. Mineralogy

The proportion of LTA for each of the coal bench samples studied is slightly higher than the respective high-temperature ash yield (Figure 14). The difference is in part due to dehydration of the clay minerals, oxidation of the pyrite, and conversion of the bassanite-forming components to either anhydrite or lime during the (high-temperature) ashing process. Different mineral assemblages occur in the LTA residues of the three coal bench samples (Table 9). The LTA of the uppermost bench mainly contains kaolinite, pyrite, illite and iron III hydroxyl-sulfate, with minor proportions of quartz, and szomolnokite, and traces of jarosite, anatase and bassanite. Minerals in the LTA of the middle bench are mainly kaolinite, with minor proportions of illite, pyrite, quartz, chlorite and bassanite, along with traces of iron III hydroxyl-sulfate, jarosite, anatase and calcite. The LTA of the lower bench is composed of kaolinite, illite, mixed-layer illite/smectite, quartz, and traces of iron III hydroxyl-sulfate, pyrite, bassanite and anatase.

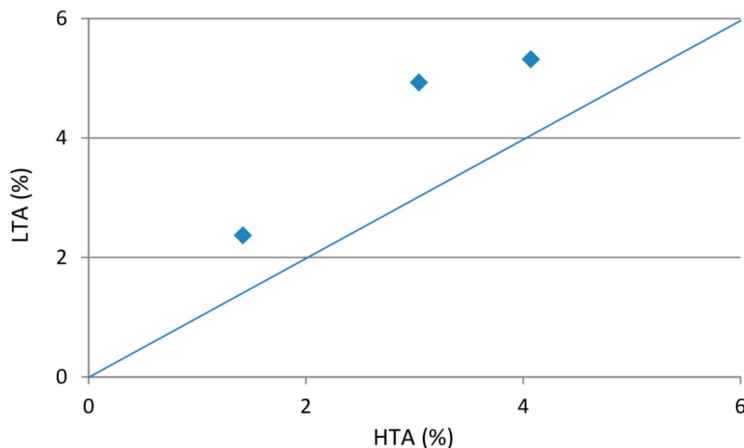


Figure 14. Relationship between low-temperature and high-temperature ash yields.

Table 9. Minerals in the coal low-temperature ashes (LTA) (A) and in whole-coal samples (B) wt %.

Sample	LTA	Quartz	Kaolinite	Illite	I/S	Chlorite	Pyrite	Iron-HS	Jarosite	Szomolnokite	Anatase	Calcite	Bassanite
A-Low-Temperature Ashes													
5508	5.3	6.7	29.2	15.6			27.2	11.8	1.6	4.5	0.6		2.7
5509	2.4	5.3	63.6	9.3		5.1	6.0	1.7	0.8		1.2	0.3	6.7
5510	4.9	17.1	45.1	19.2	12.8		0.3	1.6			0.8		3.0
B-Whole Coal													
5508	-	0.36	1.55	0.83	0.00	0.00	1.44	0.63	0.08	0.24	0.03	0.00	0.14
5509	-	0.13	1.53	0.22	0.00	0.12	0.14	0.04	0.02	0.00	0.03	0.01	0.16
5510	-	0.84	2.21	0.94	0.63	0.00	0.01	0.08	0.00	0.00	0.04	0.00	0.15

Iron-HS, Iron III hydroxyl-sulfate.

The bassanite in coal LTAs is commonly thought to be formed as an artifact of the plasma-ashing process, derived from interaction of non-mineral Ca and sulfur released from the maceral components during oxidation [106–108]. In some cases, however, the bassanite may be produced when sulfuric acid from oxidation of pyrite during storage of the coal reacts with calcite (if present) to form gypsum, which is then partly dehydrated during the low-temperature ashing process [109].

SEM-EDS studies show that the kaolinite mainly occurs in cell-fillings, indicating an authigenic origin (Figure 15A,B), although in some cases, it also occurs as massive material in the collodetrinite, most likely of detrital origin. (Figure 15E). Illite is distributed along bedding planes (Figure 15C,D), or occurs in lath form (Figure 15D,E), respectively indicating an authigenic origin and derivation from detrital materials of terrigenous origin [110,111]. Chlorite occurs in association with illite along bedding planes, suggesting a detrital origin. Quartz occurs as detrital grains in collodetrinite (Figure 15E,F). Pyrite, mainly concentrated in the top bench, occurs as framboidal and dispersed fine-grained particles in the collodetrinite (Figure 16A,B), both occurrences indicative of an authigenic origin. Anatase occurs in cell-fillings of the coal-forming plants (Figure 16C), indicating an authigenic origin. Traces of sphalerite and chalcopyrite, which are the carriers of relatively high Zn and Cu concentrations in the samples, occur in the collodetrinite of sample 5510 (Figure 15B).

A trace of an Fe-bearing phase without S, possibly an iron oxide or hydroxy-oxide (such as hematite or goethite), was detected by SEM-EDS in sample 5510 but is below the detection limit of the XRD technique. The modes of occurrence of this Fe-bearing phase, including fracture-fillings (Figure 17A),

cell-fillings (Figure 17C,D), and fine particles distributed in the collodetrinite (Figure 17D,E), indicate an epigenetic origin.

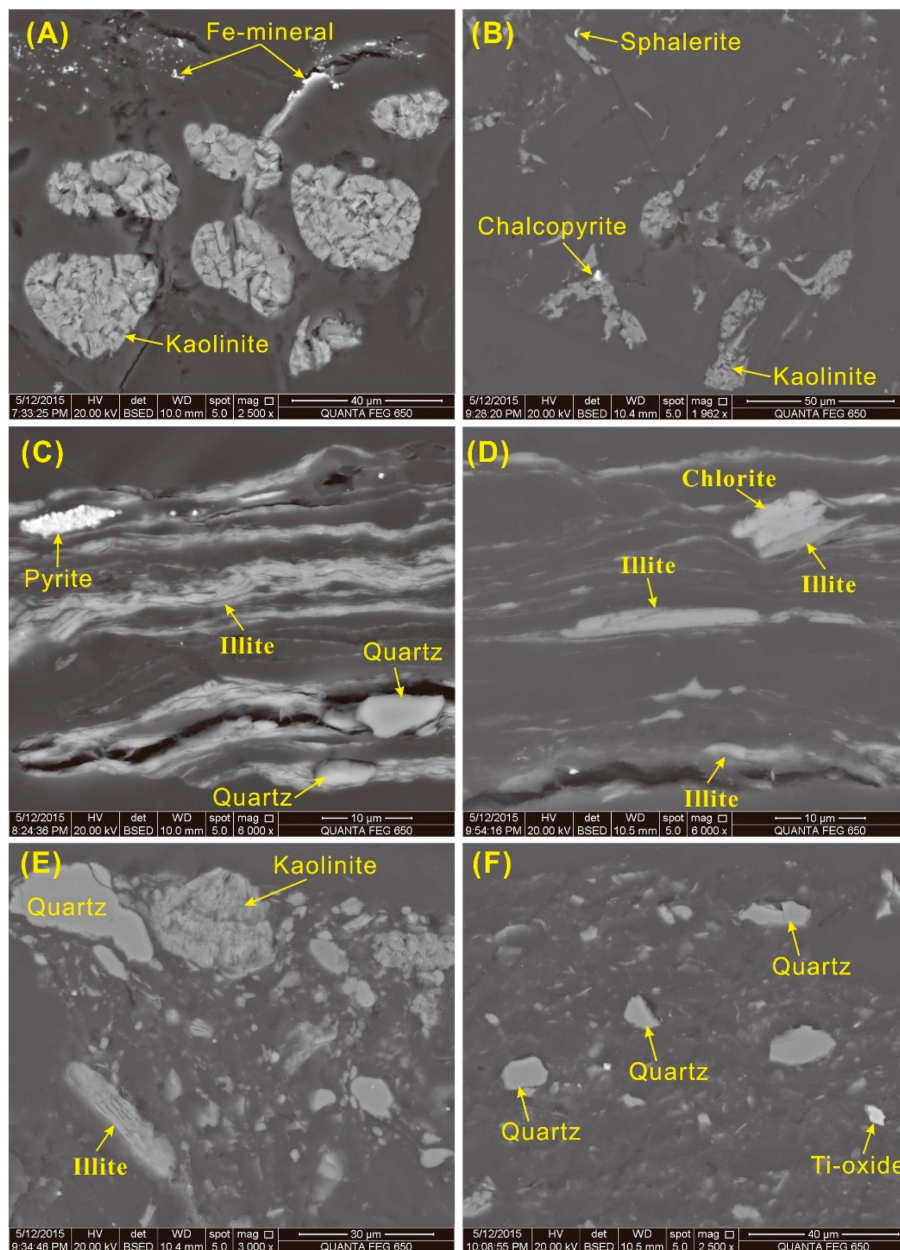


Figure 15. Back-scattered electron images of kaolinite, illite and quartz in the coal. (A) Kaolinite in cell-fillings, sample 5508; (B) Kaolinite in cell-fillings, and chalcopyrite and sphalerite in collodetrinite of sample 5510; (C) Illite distributed along bedding planes, as well as pyrite and quartz in collodetrinite, sample 5508; (D) Illite and chlorite occurring in lath form in collodetrinite, sample 5510; (E) Discrete quartz, massive kaolinite, and lath-like illite in collodetrinite, sample 5510; (F) Discrete quartz in collodetrinite, sample 5510.

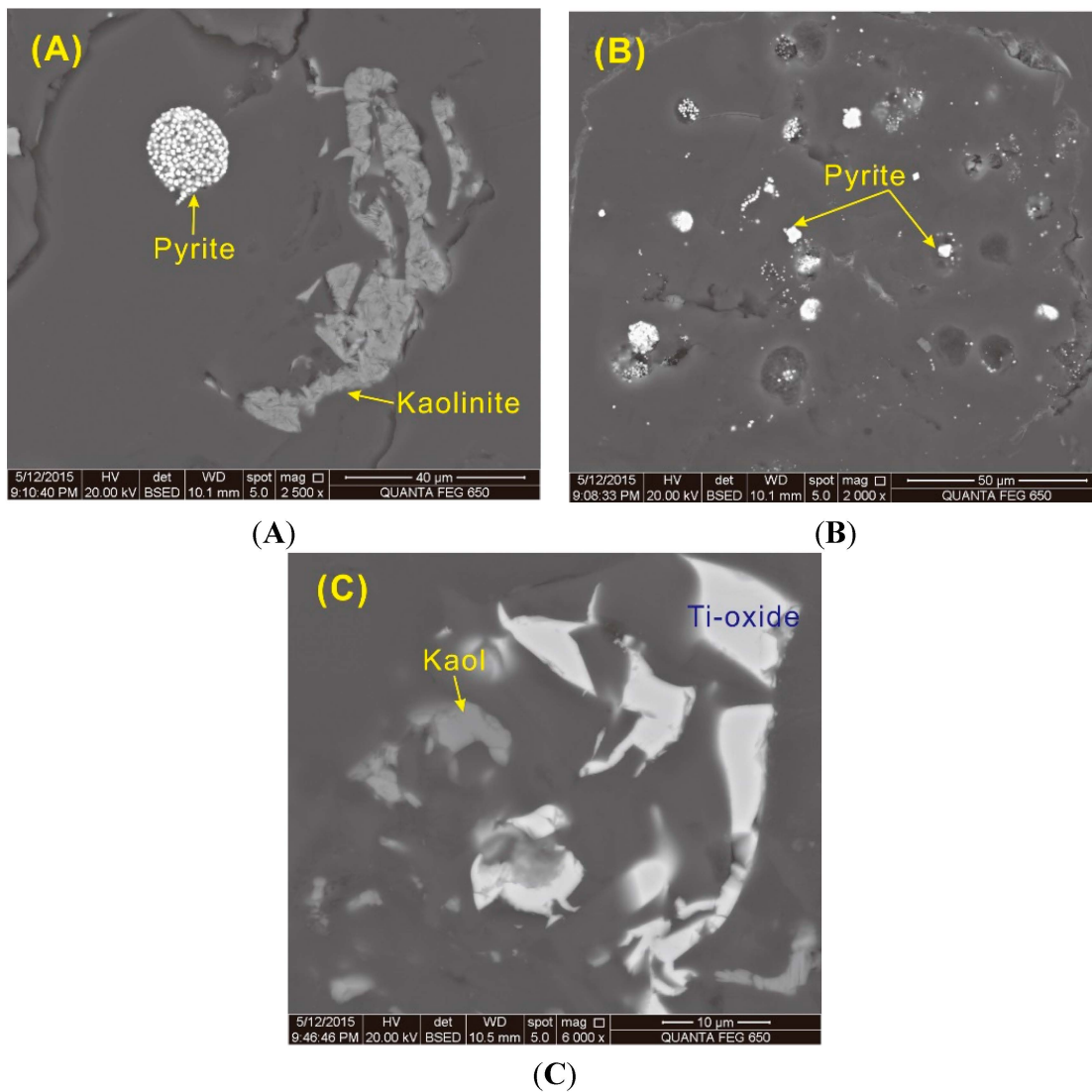


Figure 16. Back-scattered electron images of pyrite, rutile, and kaolinite in the coal. (A) Framboidal pyrite and cell-filling pyrite in sample 5509; (B) Cell-filling and dispersed pyrite in sample 5509; (C) Cell-filling anatase and kaolinite in sample 5510.

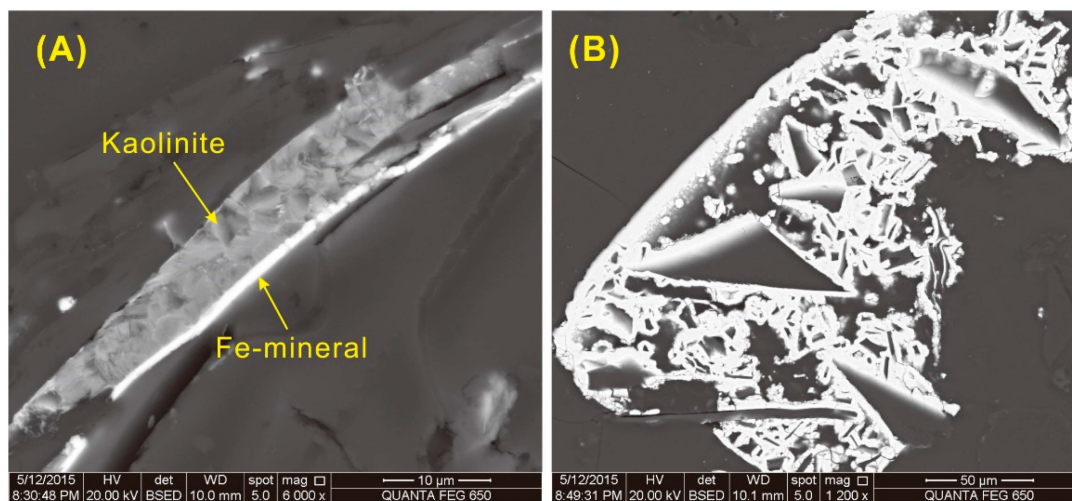


Figure 17. Cont.

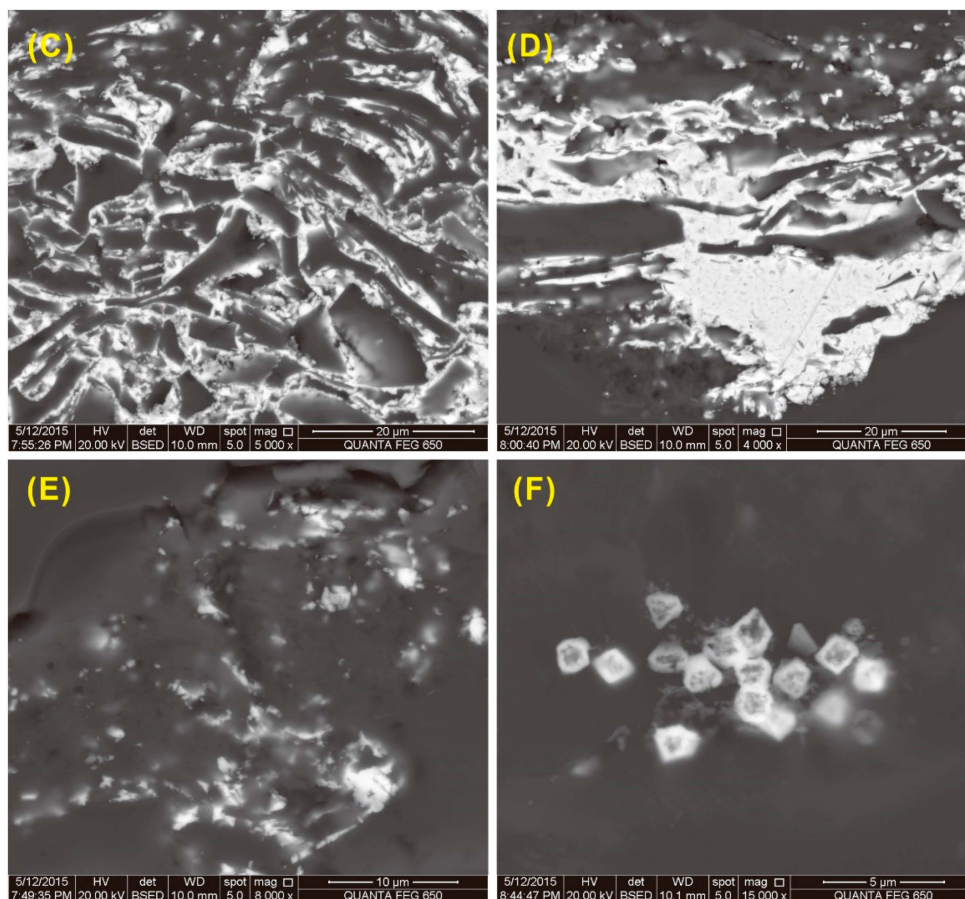


Figure 17. Back-scattered electron images of iron oxide or hydroxy-oxide (such as hematite or goethite; light-colored) in sample 5508. (A) Fe-mineral and kaolinite in fractures. (B–D), Fe-mineral in fractures. (E–F), Fe-mineral organic matter matrix.

5. Summary

The Langsettian-age high volatile A bituminous Gray Hawk coal is a relatively thin, low-S, low-ash coal that has been mined near the western margin of the Eastern Kentucky coalfield. The maceral assemblages are dominated by the vitrinite macerals collotelinite, telinite, and vitrodetrinite; and in lesser amounts, inertinite macerals fusinite + semifusinite, fecal pellet-derived macrinite, and micrinite; as well as the liptinites sporinite and cutinite. The decrease in fusinite + semifusinite from the bottom to middle benches followed by an increase in fusinite + semifusinite in the top bench is an indicator of the cycle of relatively dry vs. wet conditions during deposition of the Gray Hawk peat. The palynomorph assemblages are dominated by varieties of *Lycospora*.

The element associations in the coals (e.g., $\text{Al}_2\text{O}_3/\text{TiO}_2$, Cr/Th-Sc/Th) suggest a sediment source region dominantly comprising intermediate and felsic compositions. High As and Hg concentrations in the upper bench coincide with an increase in pyrite concentration, confirming a sulfide association.

On an ash basis, the Gray Hawk coal is significantly enriched in Ge relative to world hard coals [81], although the concentration of 569 ppm in the ash of sample 5510 is lower than that of the commercial coal-hosted Ge deposits at Lincang and Wulantuga in China and Spetuzgli in Russia. The Ga concentration on an ash-basis in the Gray Hawk coal exceeds the concentration in the fly ash from

the Al-Ga ore at Jungar, Inner Mongolia, China. The total rare earth elements plus yttrium (REY) concentrations are in excess of 1000 ppm (ash basis), making them of interest for potential industrial use.

Acknowledgments

The analyses of trace elements and mineral compositions were supported by the National Key Basic Research Program of China (No. 2014CB238902) and the National Natural Science Foundation of China (No. 41420104001). Thanks are given to Hongjian Song for his help with the low temperature ashing of coal samples.

Author Contributions

James C. Hower collected samples 5508-5510. James C. Hower and Jennifer M.K. O’Keefe were responsible for the petrology and the interpretation of the petrology. Cortland F. Eble was responsible for the palynology. Shifeng Dai, Peipei Wang, Panpan Xie and Jingjing Liu were responsible for the geochemical analyses at CUMT—Beijing. Colin R. Ward and David French were responsible for mineralogy.

Conflicts of Interest

The authors declare no conflict of interest.

References

1. Eble, C.F.; Hower, J.C. Palynologic, petrographic, and geochemical characteristics of the Manchester coal bed in eastern Kentucky. *Int. J. Coal Geol.* **1995**, *27*, 249–278. [[CrossRef](#)]
2. Hower, J.C.; Misz-Keenan, M.; O’Keefe, J.M.K.; Mastalerz, M.; Eble, C.F.; Garrison, T.M.; Johnston, M.N.; Stucker, J.D. Macrinite forms in Pennsylvanian coals. *Int. J. Coal Geol.* **2013**, *116–117*, 172–181. [[CrossRef](#)]
3. Hower, J.C.; O’Keefe, J.M.K.; Eble, C.F.; Raymond, A.; Valentim, B.; Volk, T.J.; Richardson, A.R.; Satterwhite, A.B.; Hatch, R.S.; Stucker, J.D.; *et al.* Notes on the origin of inertinite macerals in coal: Evidence for fungal and arthropod transformations of degraded macerals. *Int. J. Coal Geol.* **2011**, *86*, 231–240. [[CrossRef](#)]
4. Crowder, D.F. *Geology of the Parrot Quadrangle, Kentucky*; U.S. Geologic Quadrangle Map GQ–236; Geological Survey: Washington, D.C., USA, 1963.
5. Weir, G.W.; Mumma, M.D. *Geologic Map of the McKee Quadrangle, Jackson and Owsley Counties, Kentucky*; Geologic Quadrangle Map GQ–236; U.S. Geological Survey: Washington, D.C., USA, 1973.
6. Greb, S.F.; Eble, C.F.; Chesnut, D.R., Jr. Comparison of the Eastern and Western Kentucky coal fields (Pennsylvanian), USA—Why are coal distribution patterns and sulfur contents so different in these coal fields? *Int. J. Coal Geol.* **2002**, *50*, 89–118. [[CrossRef](#)]
7. Rimmer, S.M.; Hower, J.C.; Moore, T.A.; Esterle, J.S.; Walton, R.L.; Helfrich, C.T. Petrography and palynology of the Blue Gem coal bed, southeastern Kentucky, USA. *Int. J. Coal Geol.* **2000**, *42*, 159–184. [[CrossRef](#)]

8. Hower, J.C.; Bland, A.E. Geochemistry of the Pond Creek coal bed, Eastern Kentucky coalfield. *Int. J. Coal Geol.* **1989**, *11*, 205–226. [[CrossRef](#)]
9. Helfrich, C.T.; Hower, J.C. Palynologic and petrographic variation in the Pond Creek coal bed, Pike County, Kentucky. *Org. Geochem.* **1991**, *17*, 153–159. [[CrossRef](#)]
10. Hower, J.C.; Pollock, J.D.; Griswold, T.B. Structural controls on petrology and geochemistry of the Pond Creek coal bed, Pike and Martin Counties, eastern Kentucky. In *Geology in Coal Resource Utilization*; Peters, D.C., Ed.; American Association of Petroleum Geologists, Energy Minerals Division: Tulsa, OK, USA, 1991; pp. 413–427.
11. American Society for Testing and Materials (ASTM) International. *Test Method for Moisture in the Analysis Sample of Coal and Coke*; ASTM D3173-11; ASTM International: West Conshohocken, PA, USA, 2011.
12. American Society for Testing and Materials (ASTM) International. *Test Method for Ash in the Analysis Sample of Coal and Coke*; ASTM D3174-11; ASTM International: West Conshohocken, PA, USA, 2011.
13. American Society for Testing and Materials (ASTM) International. *Test Method for Volatile Matter in the Analysis Sample of Coal and Coke*; ASTM D3175-11; ASTM International: West Conshohocken, PA, USA, 2011.
14. American Society for Testing and Materials (ASTM) International. *Test Methods for Total Sulfur in the Analysis Sample of Coal and Coke*; ASTM D3177-02; ASTM International: West Conshohocken, PA, USA, 2002.
15. American Society for Testing and Materials (ASTM) International. *Standard Test Method for Forms of Sulfur in Coal*; ASTM D2492-02; ASTM International: West Conshohocken, PA, USA, 2002.
16. American Society for Testing and Materials (ASTM) International. *Standard Practice for Ultimate Analysis of Coal and Coke*; ASTM D3176-15; ASTM International: West Conshohocken, PA, USA, 2015.
17. American Society for Testing and Materials (ASTM) International. *Standard Test Method for Gross Calorific Value of Coal and Coke*; ASTM D5865-13; ASTM International: West Conshohocken, PA, USA, 2013.
18. Dai, S.; Wang, X.; Zhou, Y.; Hower, J.C.; Li, D.; Chen, W.; Zhu, X. Chemical and mineralogical compositions of silicic, mafic, and alkali tonsteins in the late Permian coals from the Songzao Coalfield, Chongqing, Southwest China. *Chem. Geol.* **2011**, *282*, 29–44. [[CrossRef](#)]
19. Li, X.; Dai, S.; Zhang, W.; Li, T.; Zheng, X.; Chen, W. Determination of As and Se in coal and coal combustion products using closed vessel microwave digestion and collision/reaction cell technology (CCT) of inductively coupled plasma mass spectrometry (ICP-MS). *Int. J. Coal Geol.* **2014**, *124*, 1–4. [[CrossRef](#)]
20. Taylor, J.C. Computer programs for standard less quantitative analysis of minerals using the full powder diffraction profile. *Powder Diffr.* **1991**, *6*, 2–9. [[CrossRef](#)]
21. Rietveld, H.M. A profile refinement method for nuclear and magnetic structures. *J. Appl. Crystallogr.* **1969**, *2*, 65–71. [[CrossRef](#)]

22. Ward, C.R.; Spears, D.A.; Booth, C.A.; Staton, I.; Gurba, L.W. Mineral matter and trace elements in coals of the Gunnedah Basin, New South Wales, Australia. *Int. J. Coal Geol.* **1999**, *40*, 281–308. [[CrossRef](#)]
23. Ward, C.R. Mineralogical analysis in hazard assessment. In *Geological Hazards—The Impact to Mining*; Doyle, R., Moloney, J., Eds.; Coalfield Geology Council of New South Wales: Newcastle, Australia, 2001; pp. 81–88.
24. Ruan, C.-D.; Ward, C.R. Quantitative X-ray Powder Diffraction analysis of clay minerals in Australian coals using Rietveld methods. *Appl. Clay Sci.* **2002**, *21*, 227–240. [[CrossRef](#)]
25. International Committee for Coal Petrology (ICCP). The new vitrinite classification (ICCP System 1994). *Fuel* **1998**, *77*, 349–358.
26. International Committee for Coal Petrology (ICCP). The new inertinite classification (ICCP System 1994). *Fuel* **2001**, *80*, 459–471.
27. Eble, C.F.; Gastaldo, R.A.; Demko, T.M.; Liu, Y. Coal compositional changes along a mire interior to mire margin transect in the Mary Lee coal bed, Warrior Basin, Alabama, USA. *Int. J. Coal Geol.* **1994**, *26*, 43–62. [[CrossRef](#)]
28. Hower, J.C.; Pollock, J.D. Petrology of the River Gem Coal Bed, Whitley County, Kentucky. *Int. J. Coal Geol.* **1989**, *11*, 227–245. [[CrossRef](#)]
29. Sakulpitakphon, T.; Hower, J.C.; Schram, W.H.; Ward, C.R. Tracking Mercury from the Mine to the Power Plant: Geochemistry of the Manchester Coal Bed, Clay County, Kentucky. *Int. J. Coal Geol.* **2004**, *57*, 127–141. [[CrossRef](#)]
30. Mardon, S.M.; Hower, J.C. Impact of coal properties on coal combustion by-product quality: Examples from a Kentucky power plant. *Int. J. Coal Geol.* **2004**, *59*, 153–169. [[CrossRef](#)]
31. Chou, C.-L. Sulfur in coals: A review of geochemistry and origins. *Int. J. Coal Geol.* **2012**, *100*, 1–13. [[CrossRef](#)]
32. Hower, J.C.; Rimmer, S.M. Coal rank trends in the Central Appalachian coalfield: Virginia, West Virginia, and Kentucky. *Org. Geochem.* **1991**, *17*, 161–173. [[CrossRef](#)]
33. Taylor, E.L.; Taylor, T.N.; Krings, M. *Paleobotany: The Biology and Evolution of Fossil Plants*; Elsevier: Burlington, MA, USA, 2009.
34. Krings, M. Pilzreste auf und den Fiedern zweier Pteridospermen auf und in den Stefan von Blanzky-Montceau (Zentralmassiv, Frankreich). *Geol. Saxon.* **2001**, *46–47*, 189–196.
35. Stach, E. The origin of fusain. *Gluckauf* **1927**, *63*, 759.
36. Evans, W.P. The formation of fusain from a comparatively recent angiosperm. *N. Z. J. Sci. Technol.* **1929**, *11*, 262–268.
37. Scott, A.C. Observations on the nature and origin of fusain. *Int. J. Coal Geol.* **1989**, *12*, 443–475. [[CrossRef](#)]
38. Scott, A.C. The pre-quatery history of fire. *Palaeogeogr. Palaeoclim. Palaeoecol.* **2000**, *164*, 281–329. [[CrossRef](#)]
39. Scott, A.C. Coal petrology and the origin of coal macerals: A way ahead? *Int. J. Coal Geol.* **2002**, *50*, 119–134. [[CrossRef](#)]
40. Scott, A.C.; Glasspool, I.J. Charcoal reflectance as a proxy for the emplacement temperature of pyroclastic flow deposits. *Geology* **2005**, *33*, 589–592. [[CrossRef](#)]

41. Scott, A.C.; Glasspool, I.J. The diversification of Paleozoic fire systems and fluctuations in atmospheric oxygen concentration. *Proc. Natl. Acad. Sci. USA* **2006**, *103*, 10861–10865. [[CrossRef](#)] [[PubMed](#)]
42. Scott, A.C.; Glasspool, I.J. Observations and experiments on the origin and formation of inertinite group macerals. *Int. J. Coal Geol.* **2007**, *70*, 53–66. [[CrossRef](#)]
43. Scott, A.C.; Jones, T.P. The nature and influence of fire in Carboniferous ecosystems. *Palaeogeogr. Palaeoclim. Palaeoecol.* **1994**, *106*, 91–112. [[CrossRef](#)]
44. Scott, A.C.; Cripps, J.A.; Collinson, M.E.; Nichols, G.J. The taphonomy of charcoal following a recent heathland fire and some implications for the interpretation of fossil charcoal deposits. *Palaeogeogr. Palaeoclim. Palaeoecol.* **2000**, *164*, 1–31. [[CrossRef](#)]
45. McParland, L.C.; Collinson, M.E.; Scott, A.C.; Steart, D.C.; Grassineau, N.V.; Gibbons, S.J. Ferns and fires: Experimental charring of ferns compared to wood and implications for paleobiology, paleoecology, coal petrology, and isotope geochemistry. *Palaios* **2007**, *22*, 528–538. [[CrossRef](#)]
46. Hudspith, V.; Scott, A.C.; Collinson, M.E.; Pronina, N.; Beeley, T. Evaluating the extent to which wildfire history can be interpreted from inertinite distribution in coal pillars: An example from the Late Permian, Kuznetsk Basin, Russia. *Int. J. Coal Geol.* **2012**, *89*, 13–25. [[CrossRef](#)]
47. Hudspith, V.A.; Belcher, C.M.; Yearsley, J.M. Charring temperatures are driven by the fuel types burned in a peatland wildfire. *Front Plant Sci.* **2014**, *5*. [[CrossRef](#)] [[PubMed](#)]
48. Hudspith, V.A.; Rimmer, S.M.; Belcher, C.M. Latest Permian chars may derive from wildfires, not coal combustion. *Geology* **2014**, *42*, 879–882. [[CrossRef](#)]
49. Hower, J.C.; O’Keefe, J.M.K.; Wagner, N.J.; Dai, S.; Wang, X.; Xue, W. An investigation of Wulantuga coal (Cretaceous, Inner Mongolia) macerals: Paleopathology of faunal and fungal invasions into wood and the recognizable clues for their activity. *Int. J. Coal Geol.* **2013**, *114*, 44–53. [[CrossRef](#)]
50. O’Keefe, J.M.K.; Bechtel, A.; Christanis, K.; Dai, S.; DiMichele, W.A.; Eble, C.F.; Esterle, J.S.; Mastalerz, M.; Raymond, A.L.; Valentim, B.V.; *et al.* On the fundamental difference between coal rank and coal type. *Int. J. Coal Geol.* **2013**, *118*, 58–87. [[CrossRef](#)]
51. Chipman, M.L.; Hudspith, V.; Higuera, P.E.; Duffy, P.A.; Kelly, R.; Oswald, W.W. Spatiotemporal patterns of tundra fires: Late-Quaternary charcoal records from Alaska. *Biogeosci. Discuss.* **2015**, *12*, 3177–3209. [[CrossRef](#)]
52. Pujana, R.R.; Massini, J.L.G.; Brizuela, R.R.; Burrieza, H.P. Evidence of fungal activity in silicified gymnosperm wood from the Eocene of southern Patagonia (Argentina). *Geobios* **2009**, *42*, 639–647. [[CrossRef](#)]
53. Tanner, L.H.; Lucas, S.G. Degraded wood in the upper Triassic Petrified Forest Formation (Chinle Group), Northern Arizona: Differentiating Fungal Rot from Arthropod Boring. In *The Triassic System*; Tanner, L.H., Spielmann, J.A., Lucas, S.G., Eds.; New Mexico Museum of Natural History and Science Bulletin: Albuquerque, NM, USA, 2013; Volume 61, pp. 582–588.
54. Hower, J.C.; O’Keefe, J.M.K.; Watt, M.A.; Pratt, T.J.; Eble, C.F.; Stucker, J.D.; Richardson, A.R.; Kostova, I.J. Notes on the origin of inertinite macerals in coals: Observations on the importance of fungi in the origin of macrinite. *Int. J. Coal Geol.* **2009**, *80*, 135–143. [[CrossRef](#)]

55. Hower, J.C.; Ruppert, L.F. Splint coals of the Central Appalachians: Petrographic and geochemical facies of the Peach Orchard No. 3 split coal bed, southern Magoffin County, Kentucky. *Int. J. Coal Geol.* **2011**, *85*, 268–273. [[CrossRef](#)]
56. O’Keefe, J.M.K.; Hower, J.C.; Finkelman, R.B.; Drew, J.W.; Stucker, J.D. Petrographic, geochemical, and mycological aspects of Miocene coals from the Nováky and Handlová mining districts, Slovakia. *Int. J. Coal Geol.* **2011**, *87*, 268–281. [[CrossRef](#)]
57. Richardson, A.R.; Eble, C.F.; Hower, J.C.; O’Keefe, J.M.K. A critical re-examination of the petrology of the No. 5 Block coal in eastern Kentucky with special attention to the origin of inertinite macerals in the splint lithotypes. *Int. J. Coal Geol.* **2012**, *98*, 41–49. [[CrossRef](#)]
58. Edwards, D.; Selden, P.A.; Richardson, J.B.; Axe, L. Coprolites as evidence of plant-animal interaction in Siluro-Devonian terrestrial ecosystems. *Nature* **1995**, *377*, 329–331. [[CrossRef](#)]
59. Edwards, D.; Selden, P.A.; Axe, L. Selective Feeding in an Early Devonian Terrestrial Ecosystem. *Palaios* **2012**, *27*, 509–522. [[CrossRef](#)]
60. Honegger, R.; Axe, L.; Edwards, D. Bacterial Epibionts and Endolichenic Actinobacteria and Fungi in the Lower Devonian Lichen *Chlorolichenomycites salopensis*. *Fungal Biol.* **2013**, *117*, 512–518. [[CrossRef](#)] [[PubMed](#)]
61. Cichan, M.A.; Taylor, T.N. Wood-borings in *Premnoxlon*: Plant-animal interactions in the Carboniferous. *Palaeogeogr. Palaeoclim. Palaeoecol.* **1982**, *39*, 123–127. [[CrossRef](#)]
62. Taylor, T.N.; Scott, A.C. Interactions of plants and animals during the Carboniferous. *BioScience* **1983**, *33*, 488–493. [[CrossRef](#)]
63. Dai, S.; Liu, J.; Ward, C. R.; Hower, J.C.; Xie, P.; Jiang, Y.; Hood, M.M.; O’Keefe, J.M.K.; Song, H. Petrological, geochemical, and mineralogical compositions of the low-Ge coals from the Shengli Coalfield, China: A comparative study with Ge-rich coals and a formation model for the Wulantuga Ge ore deposit. *Ore Geol. Rev.* **2015**, *71*, 318–349. [[CrossRef](#)]
64. Raymond, A.; Cutlip, P.; Sweet, M. Rates and processes of terrestrial nutrient cycling in the Paleozoic: The world before beetles, termites, and flies. In *Evolutionary Paleoecology: The Ecological Context of Macroevolutionary Change*; Allmon, W.D., Bottjer, D.J., Eds.; Columbia University Press: New York, NY, USA, 2001; pp. 235–284.
65. Baxendale, R.W. Plant-bearing coprolites from North American Pennsylvanian coal balls. *Paleontology* **1979**, *22*, 537–548.
66. Lesnikowska, A.D. Evidence of Herbivory in Tree-Fern Petioles from the Calhoun Coal (Upper Pennsylvanian) of Illinois. *Palaios* **1990**, *5*, 76–80. [[CrossRef](#)]
67. Labandiera, C.C. Early History of Arthropod and Vascular plant associations. *Annu. Rev. Earth Planet. Sci.* **1998**, *26*, 329–377. [[CrossRef](#)]
68. Labandiera, C.C.; Kvaček, J.; Mostovski, M.B. Pollination drops, pollen, and insect pollination of Mesozoic gymnosperms. *Taxon* **2007**, *56*, 663–695. [[CrossRef](#)]
69. Peppers, R.A. Comparison of Miospore Assemblages in the Pennsylvanian System of the Illinois Basin with those in the Upper Carboniferous of Western Europe. In *Proceeding of the Ninth International Congress for Carboniferous Geology and Stratigraphy*; Sutherland, P.K., Manger, W.L., Eds.; Southern Illinois University Press: Carbondale, IL, USA, 1985; Volume 2, pp. 483–502.

70. Peppers, R.A. Palynological correlation of major Pennsylvanian (Middle and Upper Carboniferous) chronostratigraphic boundaries in the Illinois and other coal basins. *Geol. Soc. Am. Mem.* **1996**, *188*, 111.
71. Eble, C.F. Applications of coal palynology to biostratigraphic and paleoecologic analyses of Pennsylvanian coal beds. In *Predictive Stratigraphic Analysis—Concepts and Application*; Cecil, C.B., Edgar, T.N., Eds.; United States Geological Survey Bulletin: Reston, VA, USA, 1994; Volume 2110, pp. 28–32.
72. Eble, C.F. Palynostratigraphy of selected Middle Pennsylvanian coal beds in the Appalachian Basin. In *Elements of Pennsylvanian Stratigraphy, Central Appalachian Basin*; Rice, C.L., Ed.; Geological Society of America Special Paper: Boulder, CO, USA, 1994; Volume 294, pp. 55–68.
73. Eble, C.F. Paleocology of Pennsylvanian coal beds in the Appalachian Basin. In *Palynology: Principles and Applications*; Jansonius, J., McGregor, D.C., Eds.; American Association of Stratigraphic Palynologists Foundation: Salt Lake City, UT, USA, 1996; Volume 3, pp. 1143–1156.
74. Eble, C.F. Lower and lower Middle Pennsylvanian coal palynofloras, southwestern Virginia. *Int. J. Coal Geol.* **1996**, *31*, 67–114. [[CrossRef](#)]
75. Ravn, R.L. Palynostratigraphy of the Lower and Middle Pennsylvanian coals of Iowa. *Iowa Geol. Survey Tech. Paper* **1986**, *7*, 245.
76. Traverse, A. *Paleopalynology*; Unwin Hyman, Ltd.: London, UK, 1988; p. 600.
77. Balme, B.E. Fossil *in situ* spores and pollen grains: An annotated catalogue. *Rev. Palaeobot. Palynol.* **1995**, *87*, 81–323. [[CrossRef](#)]
78. Dimichele, W.A.; Phillips, T.L. Paleobotanical and paleoecological constraints on models of peat formation in the Late Carboniferous of Euramerica. *Palaeogeogr. Palaeoclim. Palaeoecol.* **1994**, *106*, 39–90. [[CrossRef](#)]
79. Rothwell, G.W. Cordaixylon dumusum (Cordaitales). II. Reproductive biology, phenology, and growth ecology. *Int. J. Plant Sci.* **1993**, *154*, 572–586. [[CrossRef](#)]
80. Dai, S.; Ren, D.; Chou, C.-L.; Finkelman, R.B.; Seredin, V.V.; Zhou, Y. Geochemistry of trace elements in Chinese coals: A review of abundances, genetic types, impacts on human health, and industrial utilization. *Int. J. Coal Geol.* **2012**, *94*, 3–21. [[CrossRef](#)]
81. Ketris, M.P.; Yudovich, Y.E. Estimations of Clarkes for carbonaceous biolithes: World average for trace element contents in black shales and coals. *Int. J. Coal Geol.* **2009**, *78*, 135–148. [[CrossRef](#)]
82. Dai, S.; Li, T.; Seredin, V.V.; Ward, C.R.; Hower, J.C.; Zhou, Y.; Zhang, M.; Song, X.; Song, W.; Zhao, C. Origin of minerals and elements in the Late Permian coals, tonsteins, and host rocks of the Xinde Mine, Xuanwei, eastern Yunnan, China. *Int. J. Coal Geol.* **2014**, *121*, 53–78. [[CrossRef](#)]
83. Dai, S.; Luo, Y.; Seredin, V.V.; Ward, C.R.; Hower, J.C.; Zhao, L.; Liu, S.; Tian, H.; Zou, J. Revisiting the late Permian coal from the Huayingshan, Sichuan, southwestern China: Enrichment and occurrence modes of minerals and trace elements. *Int. J. Coal Geol.* **2014**, *122*, 110–128. [[CrossRef](#)]

84. Erarslan, C.; Örgün, Y.; Bozkurtoğlu, E. Geochemistry of trace elements in the Keşan coal and its effect on the physicochemical features of ground- and surface waters in the coal fields, Edirne, Thrace Region, Turkey. *Int. J. Coal Geol.* **2014**, *133*, 1–12. [[CrossRef](#)]
85. Tian, C.; Zhang, J.; Zhao, Y.; Gupta, R. Understanding of mineralogy and residence of trace elements in coals via a novel method combining low temperature ashing and float-sink technique. *Int. J. Coal Geol.* **2014**, *131*, 162–171. [[CrossRef](#)]
86. Sutcu, E.C.; Karayigit, A.I. Mineral matter, major and trace element content of the Afşin–Elbistan coals, Kahramanmaraş, Turkey. *Int. J. Coal Geol.* **2015**, *144–145*, 111–129. [[CrossRef](#)]
87. Brownfield, M.E.; Affolter, R.H.; Cathcart, J.D.; Johnson, S.Y.; Brownfield, I.K.; Rice, C.A.; Zielinski, R.A. Geologic setting and characterization of coal and the modes of occurrence of selected elements from the Franklin coal zone, Puget Group, John Henry No. 1 mine, King County, Washington. *Int. J. Coal Geol.* **2005**, *63*, 247–275. [[CrossRef](#)]
88. Yudovich, Y.E.; Ketris, M.P. Arsenic in coal: A review. *Int. J. Coal Geol.* **2005**, *61*, 141–196. [[CrossRef](#)]
89. Hower, J.C.; Campbell, J.L.; Teesdale, W.J.; Nejedly, Z.; Robertson, J.D. Scanning proton microprobe analysis of mercury and other trace elements in Fe-sulfides from a Kentucky coal. *Int. J. Coal Geol.* **2008**, *75*, 88–92. [[CrossRef](#)]
90. Kolker, A. Minor element distribution in iron disulfides in coal: A geochemical review. *Int. J. Coal Geol.* **2012**, *94*, 32–43. [[CrossRef](#)]
91. Finkelman, R.B. Mode of occurrence of potentially hazardous elements in coal: Levels of confidence. *Fuel Proc. Technol.* **1994**, *39*, 21–34. [[CrossRef](#)]
92. Swaine, D.J. Why trace elements are important. *Fuel Proc. Technol.* **2000**, *65*, 21–66. [[CrossRef](#)]
93. Liu, J.; Yang, Z.; Yan, X.; Ji, D.; Yang, Y.; Hu, L. Modes of occurrence of highly-elevated trace elements in superhigh-organic-sulfur coals. *Fuel* **2015**, *156*, 190–197. [[CrossRef](#)]
94. Hower, J.C.; Ruppert, L.F.; Williams, D.A. Controls on Boron and Germanium Distribution in the Low-Sulfur Amos Coal Bed: Western Kentucky Coalfield, USA. *Int. J. Coal Geol.* **2002**, *53*, 27–42. [[CrossRef](#)]
95. Yudovich, Y.E. Notes on the marginal enrichment of Germanium in coal beds. *Int. J. Coal Geol.* **2003**, *56*, 223–232. [[CrossRef](#)]
96. Seredin, V.V.; Finkelman, R.B. Metalliferous coals: A review of the main genetic and geochemical types. *Int. J. Coal Geol.* **2008**, *76*, 253–289. [[CrossRef](#)]
97. Hayashi, K.I.; Fujisawa, H.; Holland, H.D.; Ohmoto, H. Geochemistry of ~1.9 Ga sedimentary rocks from northeastern Labrador, Canada. *Geochim. Cosmochim. Acta* **1997**, *61*, 4115–4137. [[CrossRef](#)]
98. Seredin, V.V.; Dai, S. Coal deposits as potential alternative sources for lanthanides and yttrium. *Int. J. Coal Geol.* **2012**, *94*, 67–93. [[CrossRef](#)]
99. Condie, K.C. Chemical composition and evolution of the upper continental crust: contrasting results from surface samples and shales. *Chem. Geol.* **1993**, *104*, 1–37. [[CrossRef](#)]
100. Condie, K.C.; Wronkiewicz, D.J. The Cr/Th ratio in Precambrian pelites from the Kaapvaal Craton as an index of craton evolution. *Earth. Planet. Sci. Lett.* **1990**, *97*, 256–267. [[CrossRef](#)]

101. Taylor, S.R.; McLennan, S.M. *The Continental Crust: Its Composition and Evolution*; Blackwell: London, UK, 1985; p. 312.
102. Johanneson, K.H.; Zhou, X. Geochemistry of the rare earth element in natural terrestrial waters: A review of what is currently known. *Chin. J. Geochem.* **1997**, *16*, 20–42. [[CrossRef](#)]
103. Michard, A.; Albarède, F. The REE content of some hydrothermal fluids. *Chem. Geol.* **1986**, *55*, 51–60.
104. Dai, S.; Seredin, V.V.; Ward, C.R.; Jiang, J.; Hower, J.C.; Song, X.; Jiang, Y.; Wang, X.; Gornostaeva, T.; Li, X.; *et al.* Composition and modes of occurrence of minerals and elements in coal combustion products derived from high-Ge coals. *Int. J. Coal Geol.* **2014**, *121*, 79–97. [[CrossRef](#)]
105. Seredin, V.V. From coal science to metal production and environmental protection: A new story of success. *Int. J. Coal Geol.* **2012**, *90–91*, 1–3. [[CrossRef](#)]
106. Frazer, F.W.; Belcher, C.B. Quantitative determination of the mineral matter content of coal by a radio-frequency oxidation technique. *Fuel* **1973**, *52*, 41–46. [[CrossRef](#)]
107. Ward, C.R. Analysis and significance of mineral matter in coal seams. *Int. J. Coal Geol.* **2002**, *50*, 135–168. [[CrossRef](#)]
108. Ward, C.R.; Matulis, C.E.; Taylor, J.C.; Dale, L.S. Quantification of mineral matter in the Argonne Premium coals using interactive Rietveld-based X-ray diffraction. *Int. J. Coal Geol.* **2001**, *46*, 67–82. [[CrossRef](#)]
109. Rao, C.P.; Gluskoter, H.J. Occurrence and distribution of minerals in Illinois coals. *Illinois State Geol. Surv. Circ.* **1973**, *476*, 1–56.
110. Dai, S.; Hower, J.C.; Ward, C.R.; Guo, W.; Song, H.; O’Keefe, J.M.K.; Xie, P.; Hood, M.M.; Yan, X. Elements and phosphorus minerals in the middle Jurassic inertinite-rich coals of the Muli Coalfield on the Tibetan Plateau. *Int. J. Coal Geol.* **2015**, *144–145*, 23–47. [[CrossRef](#)]
111. Dai, S.; Wang, P.; Ward, C.R.; Tang, Y.; Song, X.; Jiang, J.; Hower, J.C.; Li, T.; Seredin, V.V.; Wagner, N.J.; *et al.* Elemental and mineralogical anomalies in the coal-hosted Ge ore deposit of Lincang, Yunnan, southwestern China: Key role of N₂–CO₂-mixed hydrothermal solutions. *Int. J. Coal Geol.* **2015**. [[CrossRef](#)]